


Propagating-spin-wave spectroscopy using inductive antennas: Conditions for unidirectional energy flow

Thibaut Devolder¹**Université Paris-Saclay, CNRS, Centre de Nanosciences et de Nanotechnologies, Palaiseau 91120, France* (Received 12 June 2023; revised 16 August 2023; accepted 18 October 2023; published 28 November 2023)

Many recent papers report on the interest in spin waves for applications. This paper revisits propagating-spin-wave spectroscopy when using inductive transceivers connected to a vector network analyzer. The spin-wave conduit can be made of a nonreciprocal material. The formalism offers a simple and direct method to understand, design, and optimize devices harnessing propagating spin waves, including when a unidirectional energy flow is desired. The concept of the mismatch of helicity between the spin wave and the magnetic field radiated by antennas is first clarified. Owing to the form of the susceptibility tensor reflecting the precession ellipticity, there exist specific orientations of the wave vector for which a perfect helicity mismatch is reached. The spin waves with this orientation and this direction of wave vector are “dark” in the sense that they do not couple with the inductive antenna. This leads to single-sided wave-vector generation, which should not be confused with a unidirectional emission of energy. A method to calculate the antenna-to-antenna transmission parameter is then provided. Analytical approximations are then applied on situations that illustrate the respective role of the direction of the spin-wave wave vector versus that of the group velocity. The often-encountered cases of spin waves possessing either a V-shaped or a flat dispersion relation are revisited. These reciprocal dispersion relations lead to amplitude nonreciprocity because of the helicity mismatch phenomenon. Conversely, for spin waves with a line-shaped dispersion relation, an unforeseen quasi-unidirectional emission of spin waves occurs, which is of interest for applications. This situation can be obtained when using the acoustic spin waves of synthetic antiferromagnets when the wave vector is close to parallel to the applied field. We finally show that this configuration can be harnessed to design reconfigurable frequency filters.

DOI: [10.1103/PhysRevApplied.20.054057](https://doi.org/10.1103/PhysRevApplied.20.054057)

I. INTRODUCTION

Spin waves are the resonant low-energy disturbances of the ferromagnetic order. First implemented 20 years ago [1] in the frequency domain, propagating-spin-wave spectroscopy is now a widely used technique [2] either as a research tool to access fundamental properties like the spin polarization in metals [3] and the spin-wave band structure [4], or for various practical applications [5] including novel computing schemes [6–8] or signal filtering [9]. Spin waves can be generated or amplified as soon as a torque is applied to the magnetization: spin-orbit torques [10], magnetoelastic torques [11], etc. Since the excitation of spin waves by Zeeman torques and the detection of spin waves by classical induction using simple inductive antennas is the reference method to which other schemes are most often compared [12], it is of utmost importance to describe this process exactly with a transparent formalism.

Unfortunately the published descriptions of inductive propagating spectroscopy are incomplete. Some studies focus on the emission [13,14] of spin waves in specific materials [15]. Some others use models customized for a specific configuration [16–18]. The studies sometimes disregard one component of the exciting field [19] and/or of the spin-wave stray field [20]. Finally, they often make strong assumptions on the material properties [21] to get physically sound formulas of very relevant practical interest [7,19,22] but of limited validity because their prediction accuracy is difficult to anticipate. Besides, these models cannot be applied to systems in which the spin waves exhibit a strong nonreciprocity, such as the dipolarly coupled bilayers [9] or the synthetic antiferromagnets [23–27].

A notable exception is the recent work of Weiss *et al.* [28] in which a comprehensive self-consistent theory is developed, including almost all the physical phenomena present in a propagating-spin-wave spectroscopy experiment. While this theory may be regarded as complete, it relies on a heavy mathematical formalism, which hinders

*thibaut.devolder@u-psud.fr

the physical understanding. Besides, the model must be implemented numerically, which prevents one from solving inverse problems. The available hierarchy of models is *de facto* not adequate to fully answer basic questions such as these: How does one design a transceiver that generates spin waves with positive wave vectors only? Or how does one design a system that generates spin waves carrying energy in a unique direction?

In this work, we substantially upgrade the previous versions of a formalism [4,21] to provide a comprehensive but still simple and efficient method to model and understand inductive devices harnessing propagating spin waves. We provide physically transparent formulas at the cost of minor approximations. This formalism enables one to discern the unique possibilities offered by systems whose spin waves have a linear dispersion relation: the possibility for a unidirectional flow of the spin-wave energy, and to additionally tailor its frequency response for frequency filtering.

This paper is organized as follows. Section II revisits an apparently simple problem: the magnetic field generated by a single-wire antenna and how it excites magnetization precession. A reciprocal-space analysis leads to a proper definition of the concept of helicity match or mismatch. We then analyze the stray field emitted by a spin-wave texture and how it couples to a wire antenna used as an inductive detector. We evidence that some spin waves do not emit stray field on one side of the film, such that inductive detection is rigorously blind to these “dark” modes (Sec. III). We then combine emission, propagation, and detection to issue the formalism enabling the calculation of antenna-to-antenna transmission coefficients (Sec. IV).

In the second part of the paper, we apply this formalism to paradigmatic situations. Section V shows the results for spin waves possessing a line-shaped dispersion relation and a diagonal susceptibility tensor. Section VI reports a useful lemma that is required to account for other dispersion relations. Section VII considers V-shaped dispersion relations, still with a diagonal susceptibility tensor. Then Sec. VIII accounts for the full susceptibility tensor; Sec. IX identifies to what extent this modifies the antenna-to-antenna transmission for all the previously considered dispersion relations. Finally, Secs. X and XI discuss the results and propose how to combine the single-sided wave-vector emission together with the unidirectional energy flow, in order to design novel frequency filters. The appendixes gather calculation details as well as the specific case of a flat-shaped dispersion relation.

II. THE EXCITATION PROBLEM

Let us first revisit the apparently simple problem of how the magnetic field generated by a single-wire antenna excites the magnetization of a film underneath.

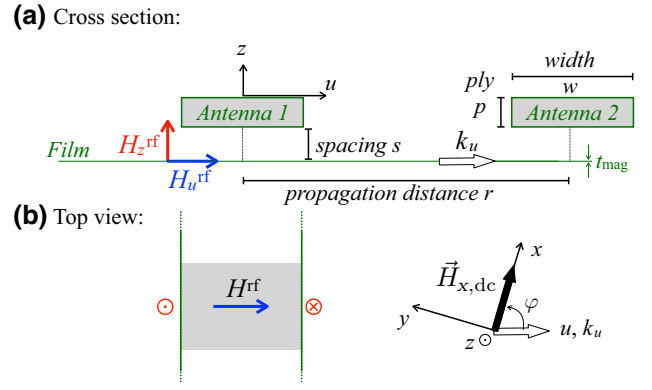


FIG. 1. (a) Cross-section view of the geometry assumed for a propagating-spin-wave spectroscopy experiment, with the definitions of the main geometrical parameters. (b) Top view with the orientation of the static field $\vec{H}_{x,dc}$ and the spin-wave wave vector \vec{k} with mutual orientation $\varphi = \{\vec{k}, \vec{H}_{x,dc}\}$.

A. Antenna field in real space

We consider a single-wire antenna whose geometry is described in Fig. 1(a). It features a rectangular cross section with a width w along the \vec{u} axis and a thickness p along the \vec{z} axis, placed at a spacing s above the mid-plane of the magnetic film. In the following, we use the $\{u, v, z\}$ coordinates when referring to the antennas, which will couple to spin waves of wave vectors k oriented in the direction u . The system is assumed invariant (and infinite) in the v direction. We will use the $\{x, y, z\}$ coordinates when dealing with magnetization dynamics, with x being the direction of the static applied field $\vec{H}_{x,dc}$. We define the angle φ between the spin-wave wave vector \vec{k} and the applied field $\vec{H}_{x,dc}$ [see Fig. 1(b)]. The antenna carries an rf current I^{rf} .

Before calculating the spatial profile of the magnetic field generated by the antenna, it is worth exploiting the symmetries of our geometry. Indeed, in all situations in which (i) the magnetostatic problem is invariant in the third direction (here invariant along $\vec{v} = \vec{e}_z \times \vec{u}$) and (ii) the sources of the magnetic field, i.e., the electrical currents and the magnetic moments, are all in the half plane below or above (in the sense of the z coordinate) the considered position (u, z) of interest, the two components of the antenna field are mutually linked [29] by a Hilbert transformation with respect to the variable u :

$$\begin{aligned} H_z^{rf}(u, z) &= -\mathcal{HT}\{H_u^{rf}(u)\} \operatorname{sgn}(z), \\ H_u^{rf}(u, z) &= \mathcal{HT}\{H_z^{rf}(u)\} \operatorname{sgn}(z). \end{aligned} \quad (1)$$

Here “sgn” is the signum function and $\mathcal{HT}\{f(\Omega)\}$ denotes the Hilbert transform of the function f of variable Ω . In our case, the sources of the magnetic field (i.e., the antenna) are above the positions of interest where the field is evaluated.

One thus takes $\text{sgn}(z) < 0$ when considering a position $\{u, z\}$ within the magnetic film.

A classical integration of the Biot-Savart law provides the in-plane field $H_u^{\text{rf}}(u, z)$ and the out-of-plane field $H_z^{\text{rf}}(u, z)$ that the antenna generates [30]. Examples of the field profiles are reported in Fig. 2(a). The expressions for the two field components are heavy and therefore placed in Appendix A [see Eqs. (A1) to (A4)]. For a didactic purpose, we first use the limit of these fields in the case of an ultrathin antenna ($p \rightarrow 0_+$) carrying the same total current. In that limit the two components of the antenna field simplify to [31]

$$\begin{aligned} \mu_0 H_u^{\text{rf}}(u, z, p \rightarrow 0) \\ = \Sigma \left[\tan^{-1} \left(\frac{w - 2u}{2z} \right) + \tan^{-1} \left(\frac{w + 2u}{2z} \right) \right] \end{aligned} \quad (2)$$

and

$$\mu_0 H_z^{\text{rf}}(u, z, p \rightarrow 0) = \frac{\Sigma}{2} \ln \left(\frac{(u - \frac{1}{2}w)^2 + z^2}{(u + \frac{1}{2}w)^2 + z^2} \right), \quad (3)$$

where $\Sigma = (1/(2\pi))(\mu_0 I^{\text{rf}}/w)$ is a scaling factor that has the dimension of a flux density (in teslas). Equations (2) and (3) can be checked [32] to comply with Eq. (1). The Hilbert transformations in Eq. (1) mean that the two components of the antenna field have correlated spatial variations. Their spectra in the reciprocal-space direction k are thus also intimately related.

B. Antenna fields in reciprocal space

We use the unitary Fourier transform convention adapted for propagating waves: for any function f , we define its spatial inverse Fourier transform as

$$\tilde{f}(k, t) = \frac{1}{\sqrt{2\pi}} \int_{-\infty}^{\infty} F(u, t) e^{i(\omega t - ku)} du.$$

We use the tilde $\tilde{}$ over a character to indicate that a quantity has a complex value. Using the properties of the Fourier transforms of two functions linked by a Hilbert transformation [Eq. (1)], we find that the inverse Fourier transforms $\tilde{h}_u^{\text{rf}}(k) = \mathcal{F}\{H_u^{\text{rf}}(u)\}$ and $\tilde{h}_z^{\text{rf}}(k) = \mathcal{F}\{H_z^{\text{rf}}(u)\}$ of the two components of the antenna field obey, for any antenna thickness,

$$\begin{aligned} \tilde{h}_z^{\text{rf}}(k) &= i \text{sgn}(kz) \tilde{h}_u^{\text{rf}}(k), \\ \tilde{h}_u^{\text{rf}}(k) &= -i \text{sgn}(kz) \tilde{h}_z^{\text{rf}}(k). \end{aligned} \quad (4)$$

Note that Eq. (4) was also derived in Refs. [13,14] and the importance of the k -odd character of $\tilde{h}_z^{\text{rf}}(k)$ was highlighted.

We emphasize that Eq. (4) means that the two components of the antenna field have the *same* power. Neglecting

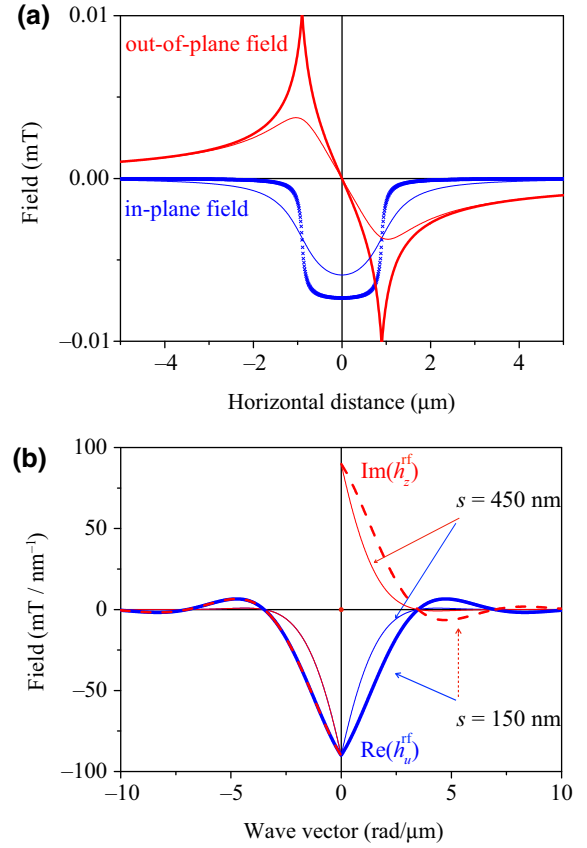


FIG. 2. (a) Real-space and (b) reciprocal-space profiles of the antenna field along a film placed below the antenna ($z < 0$). Antenna thickness and width are $h = 0.16 \mu\text{m}$ and $w = 1.8 \mu\text{m}$, respectively; antenna above film with two different spacings $s = 0.15$ and $0.45 \mu\text{m}$; rf current $I^{\text{rf}} = 1 \text{ mA}$; or equivalently -13 dBm dc dissipated in an antenna of hypothetical impedance 50Ω .

one component of the antenna field would be an error. Equation (4) also means that, for each wave vector k , the corresponding antenna field is circularly polarized with respect to the u direction, with a helicity sign set by the sign of the product kz . For each k , the spatial pattern of the k -monochromatic \tilde{h}_u^{rf} is exactly the same as that of the k -monochromatic \tilde{h}_z^{rf} but displaced by a distance of $(\pi/(2|k|)) \text{sgn}(kz)$ in the u direction, as sketched in Fig. 3.

By performing an inverse Fourier transformation on Eq. (2), we can find the (real-valued) spectrum of the antenna

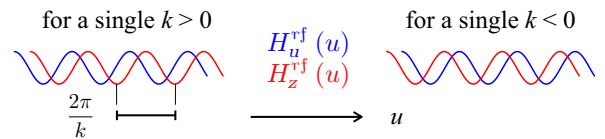


FIG. 3. Spatial profiles of the two components of the rf field of an antenna when filtered at a single wave vector.

field in the limit of $p \rightarrow 0$:

$$h_u^{\text{rf}}(k, p \rightarrow 0) = \frac{I}{2\sqrt{2\pi}} \text{sinc}\left(\frac{kW}{2}\right) e^{-|kz|} \text{sgn}(z). \quad (5)$$

The ‘‘sinc’’ in the previous expression indicates that the $h_u^{\text{rf}}(u)$ in real space resembles a rectangular window and matches with it when $p \rightarrow 0$ and $z \rightarrow 0^+$.

For an antenna of arbitrary thickness $p > 0$, a simple integration provides

$$h_u^{\text{rf}}(k, p > 0) = \frac{I}{2\sqrt{2\pi}} \text{sinc}\left(\frac{kW}{2}\right) \times \left(\frac{1 - e^{-h|k|}}{h|k|}\right) e^{-|ks|} \text{sgn}(z) \quad (6)$$

where the $\text{sgn}(z)$ should be taken as -1 since the antenna is above the film. Examples of the field profiles in reciprocal space are reported in Fig. 2(b) for representative spacings [33].

C. Linear, circular, or elliptical polarization of the antenna field in the coordinate system of the magnetization

For each wave vector, Eq. (4) means that the antenna field is circularly polarized when looked at in the coordinate system $\{\vec{u}, \vec{v}, \vec{z}\}$ common to the antenna and to the spin-wave wave vector. It is generally not the case in the frame of the film’s magnetization, since this frame is rotated by an angle φ (see Fig. 1).

When $\varphi = 0^\circ$, we have $\{\vec{x}, \vec{y}, \vec{z}\} = \{\vec{u}, \vec{v}, \vec{z}\}$. In many situations, magnets respond only to the rf fields that are in the yz plane transverse to the applied field, where the sole nonzero component is h_z^{rf} . Such magnets are thus excited by an rf field that seems *linearly polarized* along z .

In contrast, when $\varphi = 90^\circ$, we have $\{\vec{x}, \vec{y}, \vec{z}\} = \{\vec{v}, -\vec{u}, \vec{z}\}$ and the antenna field circularly polarized in the uz plane can be described with an opposite *circular polarization* in the yz plane. Using Eq. (4), we have that intermediate angles φ provide *elliptically polarized* rf fields of components:

$$\begin{aligned} \tilde{h}_z^{\text{rf}}(k) &= ih_u^{\text{rf}}(k) \text{sgn}(kz), \\ h_x^{\text{rf}}(k) &= h_u^{\text{rf}}(k) \cos(\varphi), \\ h_y^{\text{rf}}(k) &= -h_u^{\text{rf}}(k) \sin(\varphi). \end{aligned} \quad (7)$$

D. Helicity mismatch to suppress the magnetization response

The different components of the rf field [Eq. (7)] can either work together or against each other to generate spin waves, depending on whether the helicities of the rf field and of the magnetization precession match or not. Since the helicity of the antenna field depends on the sign of

k [see Eq. (4)], the degree of matching depends on the spin-wave propagation direction. This is generally seen as a difference in the efficiency of the antenna to excite the $\pm k$ counterpropagating spin waves [14], leading to some amplitude nonreciprocity.

To achieve a physically transparent description of this ‘‘helicity mismatch’’ effect, let us look at the high-frequency susceptibility tensor $\bar{\bar{\chi}}(k)$ of the total moment of a magnet system. For a didactic purpose, we temporarily disregard the fact that $\bar{\bar{\chi}}(k)$ and $\bar{\bar{\chi}} = \bar{\bar{\chi}}(k=0)$ slightly differ [34]. With an applied field along x , $\bar{\bar{\chi}}$ is generally finite only in the $\{y, z\}$ plane. In this plane it reads

$$\bar{\bar{\chi}} = \chi_{\text{max}} \begin{pmatrix} 1 & -i\epsilon \\ i\epsilon & \epsilon^2 \end{pmatrix}, \quad (8)$$

where $\chi_{\text{max}} \in i\mathbb{R}^-$ is the value of the χ_{yy} term of the susceptibility at resonance, and ϵ is the precession ellipticity.

The magnetization response $\tilde{m}^{\text{rf}}(k) = \bar{\bar{\chi}} h^{\text{rf}}(k)$ follows from Eqs. (7) and (8). The response vanishes in the ‘‘perfect’’ helicity mismatch (HMM) case. This happens for specific field directions φ , which read simply

$$\sin(\varphi_{\text{HMM}}) = \epsilon \text{sgn}(kz). \quad (9)$$

For these angles, the antenna field excites only one of the two directions of the wave vector [35]. These HMM angles depend on the precession ellipticity $\epsilon(k, H_{x,\text{dc}})$ only, which is weakly field- and wave-vector-dependent. This single-sided wave-vector generation is not to be confused with the generation of a unidirectional energy flow. This point can be very important when looking at angular variations in propagating-spin-wave spectroscopy. We will come back to this point later.

This form of $\bar{\bar{\chi}}$, in which [Eq. (8)] the nondiagonal components are shifted in phase by $\pm i$ (i.e., $\pm\pi/2$ rad) with respect to the diagonal elements, occurs in many situations [15]. It is worth noting that this includes the total moment of a synthetic antiferromagnet (SAF) at its acoustic resonance [27], which is the material system that we shall harness for the application proposed in Sec. X. In this case the precession ellipticity is $\epsilon = \sqrt{H_j} / \sqrt{H_j + M_s}$ at low fields, where we have defined the interlayer exchange field $\mu_0 H_j = -2J / (M_s(t_{\text{mag}}/2))$, with J being the interlayer exchange coupling and t_{mag} the total thickness of the SAF. In numerical applications, we shall take the material parameters of a $\text{Co}_{40}\text{Fe}_{40}\text{B}_{20}/\text{Ru}/\text{Co}_{40}\text{Fe}_{40}\text{B}_{20}$ SAF from Ref. [36], i.e., $t_{\text{mag}} = 34$ nm, $J = -1.7$ mJ/m², and $\mu_0 M_s = 1.7$ T. This leads to a precession ellipticity $\epsilon \approx 0.3$ for the acoustic spin-wave branch, so that the perfect helicity mismatch angles are $\varphi_{\text{HMM}} = 16^\circ$ or 164° for $k < 0$ and equivalently 163° or 343° for $k > 0$.

III. THE DETECTION PROBLEM

A. From the dynamic magnetization of the spin wave to its stray fields

1. Formalism

We now consider a spin wave of wave vector k with dynamical components $m_{u,v,z}(u, t) = \text{Re}(\tilde{m}_{u,v,z} e^{i[\omega t - ku]})$ with complex amplitudes $\{\tilde{m}_u, \tilde{m}_v = 0, \tilde{m}_z\}$ (in units of A/m). From now on, we postulate that the magnetization can be replaced by its thickness-averaged value. The stray field will be simpler to express in the frame of the magnetic film, so that we now take the $z' = 0$ plane as the center of the film of thickness t_{mag} . The stray field created by this spin wave can be calculated as in Ref. [37].

The \tilde{m}_u generates a volume density $\tilde{\rho}(u, z') = ik\tilde{m}_u e^{-iku}$ of magnetic pseudocharges within the magnetic body, from which the magnetostatic potential can be deduced by integration. Taking its gradient, we get that the in-plane dynamic component \tilde{m}_u of the magnetization generates a stray field outside of the film whose in-plane component is

$$H_u^{\text{stray}, m_u}(u, z') = -\tilde{m}_u e^{-|kz'|} e^{-iku} \sinh\left(\frac{kt_{\text{mag}}}{2}\right) \text{sgn}(k). \quad (10)$$

In parallel, the \tilde{m}_z component of the spin wave generates a surface density $\tilde{\sigma}(u, z') = \pm \delta_{z' \mp t/2} \tilde{m}_z e^{-iku}$ of magnetic pseudocharges at the top (+) and bottom surfaces (−) of the magnetic body, from which the corresponding magnetostatic potential can be deduced. This gives another source of in-plane-oriented stray field:

$$H_u^{\text{stray}, m_z}(u, z') = i\tilde{m}_z e^{-|kz'|} e^{-iku} \sinh\left(\frac{kt_{\text{mag}}}{2}\right) \text{sgn}(z'). \quad (11)$$

For one spin wave of wave vector k , the total stray field is the sum of these two contributions:

$$H_u^{\text{stray}}(u, z') = [i\tilde{m}_z \text{sgn}(z') - \tilde{m}_u \text{sgn}(k)] \times e^{-|kz'|} e^{-iku} \sinh\left(\frac{kt_{\text{mag}}}{2}\right). \quad (12)$$

We will see later that this u -oriented component of the dynamic stray field is the only one that matters for the inductive detection by the receiving antenna; it is, however, instructive to also have a look at the other field component.

The sources $\tilde{\rho}$ and $\tilde{\sigma}$ of the stray magnetic field are now all *below* the position of interest for detection (the antenna), such that, for the solitary spin wave of wave vector k , the spatial profile of the stray field now follows a

modified version of Eq. (4):

$$\tilde{H}_z^{\text{stray}}(u, z') = -i \text{sgn}(kz') \tilde{H}_u^{\text{stray}}(u, z'), \quad (13)$$

which [38] holds out of the film (i.e., for $|z'| \geq t_{\text{mag}}/2$) and for a single spin wave of wave vector k . An example of the stray field profile associated with a single spin wave is given in Fig. 4. We emphasize that, owing to the minus sign in Eq. (12), the amplitude of the stray field on one side of the film is stronger than that on the other side. This is particularly important when intending to detect the spin wave inductively.

2. Single-sided stray field cases versus helicity mismatch

It is interesting to scrutinize when Eqs. (12) and (13) vanish for one sign of kz' , because this means that the spin wave emits flux in one half z -space only, either above or below the film, in a manner similar to the “fridge magnet” configuration [37] approximated in Halbach linear arrays of permanent magnets [39]. As is well known, a single-sided stray field happens every time the two components of the dynamic magnetization are related by a Hilbert transformation [37], or equivalently when Eq. (13) applies for all the wave vectors present in the magnetization texture.

Going back to the frame $\{u, z\}$ that is the one relevant for the inductive detection, the components of any spin wave $\{\tilde{m}_x, \tilde{m}_y, \tilde{m}_z\}$ can be rewritten as $\tilde{m}_u = -\tilde{m}_y \sin \varphi$ and \tilde{m}_z . Equations (12) and (13) can be used to get the dynamical components of the stray field projected in the plane relevant for inductive detection. These components vanish for the no-inductive-detection (NID) condition, defined as

$$\sin \varphi_{\text{NID}} = -i \frac{\tilde{m}_z}{\tilde{m}_y} \text{sgn}(kz'). \quad (14)$$

For an antenna placed above the magnetic film ($z' > 0$ and $z < 0$), the conditions of perfect helicity mismatch [Eq. (9)] for which a spin wave of wave vector k is strictly not responding to the antenna field, and the condition [Eq. (14)] for which the same spin wave cannot be detected by the same antenna, are identical.

This intuitive conclusion can be rephrased in a simple rule: if an inductive antenna cannot excite a spin wave, it also cannot detect inductively this spin wave. This rule is not specific to inductive antennas, and was for instance also observed for transducers based on nanomagnet resonators [40–42].

B. From the stray field of the spin wave to the electromotive force

We now need to get the electromotive force (emf) that this stray field induces on the receiving inductive antenna. For a start, we consider an ultrathin and ultranarrow antenna (i.e., $p, w \rightarrow 0$). Using the Maxwell-Faraday

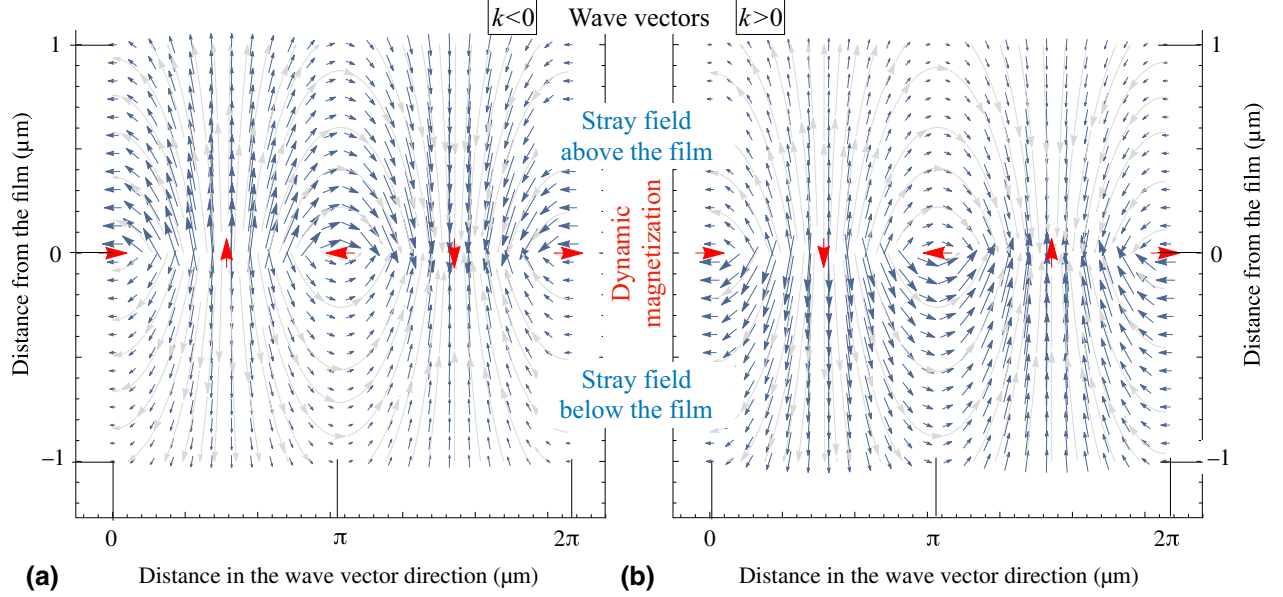


FIG. 4. Stray field outside of a thin film for counterpropagating spin waves with ellipticity such that $\tilde{m}_z = -0.3i\tilde{m}_u$, following Eqs. (12) and (13). The spin waves have a wavelength of $2\pi/k$ for $|k| = 1 \text{ rad}/\mu\text{m}$: (a) for $k < 0$, and (b) for $k > 0$. The red arrows sketch the normalized dynamic magnetic magnetization $\{\text{Re}(\tilde{m}_u e^{i(\omega t - ku)}), \text{Re}(\tilde{m}_z e^{i(\omega t - ku)})\}$ inside the film at time zero for a film of hypothetical vanishingly small thickness. The sizes of the blue arrows scale with the amplitude of the stray field (arb. units).

equation, which reads $\vec{\nabla} \times \vec{E} = -(\partial \vec{B} / \partial t)$, the time variation of the spin-wave stray field generates an electric field whose component in the \vec{v} direction is

$$\vec{E}_v(u, z', p = w = 0) = -i\omega \int_s^\infty \tilde{H}_u^{\text{stray}}(u, z') dz'. \quad (15)$$

Considering a finite-size antenna requires one to average this expression over z' spanning from s to $s + p$ and over u spanning from $-w/2$ to $w/2$. This gives a mutual inductance that scales with the emf per unit length on the receiving antenna:

$$\frac{1}{i\omega} \frac{\partial(\text{emf})}{\partial v} = \text{sinc}(kw/2) [\tilde{m}_u - i\tilde{m}_z \text{sgn}(kz')] \times \left(\frac{1 - e^{-p|k|}}{p|k|} \right) e^{-|ks|} \frac{\sinh(kt_{\text{mag}}/2)}{k}. \quad (16)$$

In practice, a typical experiment is performed with wave vectors bounded by the antenna width, i.e., $|k| < 2\pi/w$, on a device whose geometry complies with $w \gg s, p, t_{\text{mag}}$, such that the second line of Eq. (16) can be reasonably approximated by $t_{\text{mag}}/2$.

IV. THE TRANSMISSION PROBLEM

A. Contribution of the spin waves to the antenna-to-antenna scattering matrix

Let us calculate the antenna-to-antenna transmission parameter as would be measured by a vector network

analyzer (VNA) at an applied frequency $\omega/(2\pi)$. This frequency is *a priori* distinct from the uniform resonance frequency ω_0 . We start by evaluating the response at a single wave vector k . We express the antenna field at the emitter [Eqs. (6) and (4)] in the frame of the applied dc field, i.e., the $\{x, y, z\}$ frame. For an antenna placed above the film, this stimulus is $\tilde{h}h_u^{\text{rf}}(k, z)$ with h_u^{rf} from Eq. (6) and

$$\tilde{h} = (\cos(\varphi), -\sin(\varphi), -i \text{sign}(k)). \quad (17)$$

We then evaluate the magnetization response below the emitter antenna using $\tilde{m}(k)|_{u=0} = \tilde{\chi} \cdot (\tilde{h}h_u^{\text{rf}}(k))$. Note that the dynamic susceptibility $\tilde{\chi}_{(\omega, k)}$ has to be expressed for the wave vector and frequency currently under investigation, and in the $\{x, y, z\}$ frame of the magnetic field.

This dynamic response is propagated toward the receiving antenna at the position $u = r$ by a multiplication by the phase accumulation scalar term,

$$\tilde{m}(k)|_{u=r} = \tilde{m}(k)|_{u=0} e^{-ikr}.$$

Then this dynamic magnetization below the receiving antenna is reprojected in the $\{u, v, z\}$ frame of the antenna to get $(\tilde{m}_u(r), m_v(r), \tilde{m}_z(r))$, thus enabling the calculation of the emf of the receiving antenna. This expression can be simplified once one notices in Eq. (16) that the emf scales like the scalar product between the magnetization and \tilde{h}^* , where the star symbol denotes the complex conjugate. The current-in to emf-out transmission parameter as enabled by the spin waves between antenna 1 and antenna 2 reads

$$\tilde{S}_{21f}(\omega, r) \propto \int_{-\infty}^{+\infty} [\bar{h}^* \cdot [\bar{\chi}_{(\omega, k)} \cdot \bar{h}]] e^{-ikr} (h_u^{\text{rf}}(k, z))^2 dk, \quad (18)$$

where we have omitted the numerical prefactor $2\sqrt{2\pi} [(1/k) \sinh(kt_{\text{mag}}/2)]$ that is essentially independent of k but is proportional to wt_{mag} , i.e., the volume of the spin-wave conduit. The subscript label “ f ” refers to the integration over the *full* spectrum (i.e., $k \in]-\infty, +\infty[$), as opposed to the partial responses to be calculated later in this paper.

The reflection parameter S_{11f} and reverse transmission parameter S_{12f} can be calculated with the same expression but with $r = 0$ and $r < 0$. Note also that, abusing notation, we write S_{21} and S_{11} for quantities that, strictly speaking, would not be those measured with a VNA, since the VNA scattering parameters would also be functions of additional impedances within the circuit.

B. Transmission in the absence of Gilbert damping

The most trivial situation is the limit of vanishing Gilbert damping ($\alpha \rightarrow 0$) but arbitrary dispersion relation. In that case, for any applied frequency ω , there are a small number of resonant spin waves of wave vectors k_0 , each with a vanishing linewidth and a diverging susceptibility.

When $\alpha \rightarrow 0$ each resonant spin wave contributes to the susceptibility tensor by a term essentially of the form

$$\left(-i \frac{2\pi}{t_{\text{mag}}} \delta_{k_0} \pm \frac{1}{t_{\text{mag}}} \frac{1}{k - k_0} \right) \begin{pmatrix} 1 & -i\epsilon(k_0) \\ i\epsilon(k_0) & \epsilon(k_0)^2 \end{pmatrix}, \quad (19)$$

where δ is the Dirac distribution and the \pm sign is the sign of the group velocity at the considered k_0 .

The contribution of each k_0 (i.e., each pole) of the susceptibility to the antenna-to-antenna transmission coefficient can be calculated from the combination of Eqs. (18) and (19) and the residue theorem. Overall, we have

$$\tilde{S}_{21f}(\omega, r, \alpha \rightarrow 0) \propto -i \frac{4\pi}{t_{\text{mag}}} \sum_{\text{resonant } k_0\text{'s}} X_{k_0} e^{-ik_0 r} (h_u^{\text{rf}}(k_0))^2, \quad (20)$$

where X_{k_0} are helicity mismatch numerical terms that depend on the sign of each k_0 , on φ [see Eq. (17)], on the precession ellipticity, and on the peak susceptibility value. Note that Eq. (20) is the intuitive formula used in many places [4,7,19,21,42] when a qualitative understanding is sufficient. It expresses that the frequency dependence of the phase of $\tilde{S}_{21f}(\omega, r, \alpha \rightarrow 0)$ can be used to get the dispersion relation provided a single mode contributes to the transmission parameter [4]. In practice, the damping is finite and Eq. (20) has to be tested against more realistic calculations.

C. Particular cases where analytical solutions exist

Although we will often integrate Eq. (18) numerically to get exact results, it is interesting to look at situations for which $\tilde{S}_{21f}(\omega, r)$ can be calculated analytically and lead to physically transparent expressions at the cost of minor approximations.

These situations happen when the dispersion relation is line-shaped or broken-linear in the “relevant” wave vector allowed by the antenna geometry (i.e., typically for $k \in [-2\pi/w, 2\pi/w]$). The analytical calculations require the different terms of $\bar{\chi}$ to be treated one by one to circumvent the difficulty associated with the $\text{sgn}(k)$ dependence of the z component of \bar{h} within Eq. (18). We shall sort these contributions into two categories.

We will use the superscript yy in \tilde{S}_{21f}^{yy} for transmission parameters involving a diagonal term of the susceptibility matrix, leading to an integrand of Eq. (18) that is independent of $\text{sgn}(k)$. Conversely, the susceptibility terms in $[\bar{h}^* \cdot [\bar{\chi}_{(\omega, k)} \cdot \bar{h}]]$ that involve the component \bar{h}_z exactly once lead to a $\text{sgn}(k)$ dependence of the integrand within Eq. (18). For these terms, we shall use the superscript $1z$ [short for \bar{h}_z is involved exactly once].

The interesting situations are as follows (and see Fig. 5):

(a) When the dispersion relation is monotonically linear across the relevant k spectrum, and when in addition the magnetization is excited by a diagonal susceptibility term only (Sec. V). The label “ $/$ ” in $\tilde{S}_{21f}^{yy}(\omega, r, /)$ will be used to recall the line-shaped nature of the dispersion relation with a positive slope v_g , in contrast to the self-understandable other cases displayed in Fig. 5: $\tilde{S}_{21f}^{yy}(\omega, r, \setminus)$, $\tilde{S}_{21f}^{yy}(\omega, r, \vee)$, and $\tilde{S}_{21f}^{yy}(\omega, r, -)$.

(b) When the dispersion relation or the rf field are different for the two signs of k so that two partial responses must be calculated separately (to be referred to as \tilde{S}_{21+}^{yy} for $k > 0$ and \tilde{S}_{21-}^{yy} for $k < 0$, Sec. VI). The lemma of this situation [Eq. (30)] will be used extensively in the later calculations.

(c) When the dispersion relation is V-shaped and the magnetization is excited by a diagonal susceptibility term only [to be referred to as $\tilde{S}_{21f}^{yy}(\vee)$, Sec. VII].

(d) When the dispersion relation is flat and the magnet is excited by a diagonal susceptibility term only [to be referred to as $\tilde{S}_{21f}^{yy}(-)$, Appendix B].

(e) Finally, we shall derive the full response, i.e., when all susceptibility terms are included in the response [to be referred to as \tilde{S}_{21f} , first formally in Sec. VIII then case by case in Sec. IX and Appendix B 3].

From now on, we define ω_0 and $\Delta\omega_0$ as the $k = 0$ (uniform) resonance frequency and linewidth at the presently applied field. At the presently applied frequency $\omega \neq \omega_0$, there can exist resonant spin waves. Their wave vectors will be written as k_0 's.

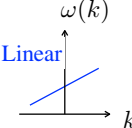
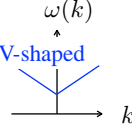
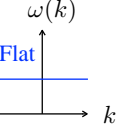
Types of dispersion relation		
 <p>Linear</p>	 <p>V-shaped</p>	 <p>Flat</p>
$\bar{\chi} = \begin{pmatrix} 1 & 0 \\ 0 & \epsilon^2 \end{pmatrix}$		
Responses for a diagonal susceptibility tensor:		
Section V $\tilde{S}_{21f}^{yy}(\omega, r, /)$ Eq. (22) Unidirectional	§ VII $\tilde{S}_{21f}^{yy}(\omega, r, \vee)$ Eqs. (35), (C1)-(C3) Reciprocal	Appendix B $\tilde{S}_{21f}^{yy}(\omega, r, -)$ Eqs. B1, B3 Non-propagative
$\bar{\chi} = \begin{pmatrix} 0 & -i\epsilon \\ i\epsilon & 0 \end{pmatrix}$		
Additional contributions for the antidiagonal parts of the susceptibility:		
Section IX.A $\tilde{S}_{21f}^{1z}(\omega, r, /)$ Eq. (38) Reduces unidirectionality	§ IX.B $\tilde{S}_{21f}^{1z}(\omega, r, \vee)$ Eq. (41) Engender amplitude non-reciprocity	Appendix B.3 $\tilde{S}_{21f}^{1z}(\omega, r, -)$ Eq. (38)

FIG. 5. Top: Types of dispersion relations (blue) for which illustrative analytical formulas are derived. Middle: Contributions of diagonal elements of the susceptibility: sections, notations, equations, and main feature (green). Bottom: Likewise for the nondiagonal elements of the susceptibility (brown).

V. LINEAR DISPERSION RELATION AND DIAGONAL SUSCEPTIBILITY: UNIDIRECTIONAL ENERGY FLOW

In this section, we assume a perfectly linear dispersion relation $\omega(k) = \omega_0 + v_g k$ with $v_g \neq 0$, valid up to the maximum wave vector compatible with the antenna geometry. In practice, this kind of dispersion relation can arise in a dipolarly coupled bilayer [9] and in a synthetic antiferromagnet [27] near $k = 0$. In the present section, we assume that the antenna is ultrathin and that it is in direct contact with the film (i.e., $s = p = 0$). We also assume that the magnet reacts to the rf field by only one of its diagonal susceptibility terms (e.g., yy); therefore, we use the notation $\tilde{S}_{21f}^{yy}(\omega, r, /)$.

At the applied frequency ω , there is a single resonant spin wave, whose wave vector is $k_0 = (\omega - \omega_0)/v_g$. The considered susceptibility term can be expanded to first order in k and written in the form [21]

$$\chi(k) = -\frac{i \Delta \omega_0 \chi_{\max}}{2v_g(k - k_0 + i/L_{\text{att}})}, \quad (21)$$

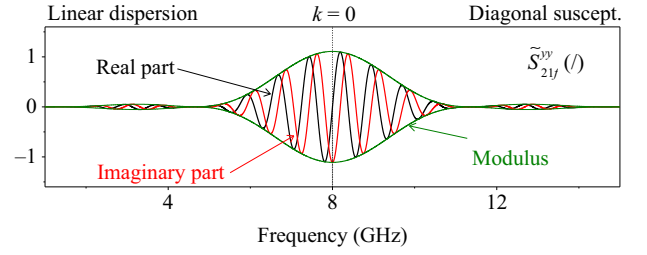


FIG. 6. Frequency dependence of the antenna-to-antenna transmission parameter $\tilde{S}_{21f}^{yy}(\omega, r = 8 \mu\text{m}, /)$ for a diagonal susceptibility term and a linear dispersion relation [Eq. (22)]. The uniform resonance is $\omega_0/(2\pi) = 8$ GHz, with $v_g = 6$ km/s and $L_{\text{att}} = 6 \mu\text{m}$. The antennas have zero thickness ($p = 0$) and are in direct contact with the film ($s = 0$). The width of the antennas is $w = 1.8 \mu\text{m}$.

where $L_{\text{att}} = 2v_g/\Delta\omega_0$ is the attenuation length [10]. Let us first consider a positive group velocity, hence $L_{\text{att}} > 0$.

A. Linear dispersion with a positive group velocity

After some algebra and using Eq. (21), one can rewrite Eq. (18) in a form containing explicitly propagating (P) and nonpropagating (L , for local) contributions, as well as a common Lorentzian-resonant prefactor $\mathcal{L}(\omega)$:

$$\tilde{S}_{21f}^{yy}(\omega, r, /) = \underbrace{\sqrt{\frac{\pi}{2}} \mathcal{L}(\omega)}_{\text{Lorentzian}} \left[\underbrace{P_1(r, \omega)}_{\text{propag.}} \underbrace{U(r)}_{\text{unidir.}} \right] \times \underbrace{-2L(r) + L(r+w) + L(r-w)}_{\text{local}}. \quad (22)$$

The frequency spectrum and the distance dependence of $\tilde{S}_{21f}^{yy}(\omega, r, /)$ are plotted in Figs. 6 and 7 for some illustrative parameters. The forms of these frequency and propagation-distance dependences can be understood by scrutinizing the different contributions within $\tilde{S}_{21f}^{yy}(\omega, r, /)$.

The complex-valued prefactor is

$$\mathcal{L}(\omega) = \frac{\chi_{\max}}{w^2} \frac{v_g^2}{(L_{\text{att}}(\omega - \omega_0) - iv_g)^2}. \quad (23)$$

This prefactor appears as a resonance centered at ω_0 and decaying with the frequency detuning $|\omega - \omega_0|$ at a rate set by the linewidth $2v_g/L_{\text{att}}$. Note that $\mathcal{L}(\omega)$ is symmetric with respect to ω_0 : the material responds also at frequencies below its uniform (i.e., $k = 0$) resonance (see Fig. 6).

This prefactor multiplies a first *propagating* term that includes a phase rotation and a spatial decay operand:

$$P_1(r, \omega) = |L_{\text{att}}| e^{ir(\omega - \omega_0)/v_g} e^{-r/L_{\text{att}}}. \quad (24)$$

The phase accumulation $e^{ir(\omega - \omega_0)/v_g}$ translates into clear oscillations of the real and imaginary parts of $\tilde{S}_{21f}^{yy}(\omega, r, /)$ as the frequency (hence k) increases; see Fig. 6. They come with an exponential spatial decay.

This operand $P_1(r, \omega)$ is multiplied by a *unidirectional* term $U(r, \omega)$ that reads

$$U(r, \omega) = -4\Theta(r) + 2 \left[\Theta_{(r-w)} \exp\left(\frac{w}{L_{\text{att}}} + \frac{iw(\omega - \omega_0)}{v_g}\right) + \Theta_{(r+w)} \exp\left(\frac{-iw(\omega - \omega_0)}{v_g} - \frac{w}{L_{\text{att}}}\right) \right]. \quad (25)$$

The Heaviside functions $\Theta(r)$, $\Theta(r - w)$, and $\Theta(r + w)$ indicate that energy is not sent in the direction *opposite* to the group velocity v_g : the term $\mathcal{L}(\omega)P_1(r, \omega)U(r)$ in Eq. (22) is finite only for $r > -w$ (see Fig. 7). The three Heaviside terms in $U(r, \omega)$ indicate that the emission can be understood as performed by the center of the antenna (accounted for by the term $\Theta(r)$), with correction terms $\Theta(r \pm w)$, accounting for the extra loss or under loss $e^{\mp w/L_{\text{att}}}$ due to the differing distances between the position of interest r and the farthest or closest antenna edges.

Finally, the expression for $\tilde{S}_{21f}^{yy}(\omega, r, /)$ includes ‘‘local terms’’ [free of the propagation-induced dephasing and free of the propagation-induced loss previously expressed in Eq. (24)]. They can be written in terms of the function

$$L(x, \omega) = \text{sgn}(x) \left(+L_{\text{att}} - x - \frac{ixL_{\text{att}}(\omega - \omega_0)}{v_g} \right). \quad (26)$$

These terms are local in the sense that their sum vanishes for $|r| > w$, as illustrated in Fig. 7 (dotted line). These

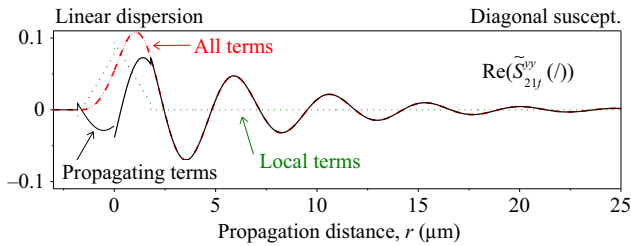


FIG. 7. Distance dependence of the different contributions to the real part of the antenna-to-antenna transmission parameter $\text{Re}(\tilde{S}_{21f}^{yy}(\omega, r, /))$ for a linear dispersion relation and a diagonal susceptibility [Eq. (22)]. The parameters are $2\pi v_g/(\omega - \omega_0) = 4.7 \mu\text{m}$, $L_{\text{att}} = 6 \mu\text{m}$, and $v_g = 6 \text{ km/s}$. The antenna geometry is $p = s = 0$ and $w = 1.8 \mu\text{m}$. Note the unidirectional character of the energy flow.

terms can be understood as the self-inductance of the emitter antenna. In practice, they matter only when calculating the reflection coefficient S_{11f}^{yy} . Importantly, the local terms preserve the unidirectional energy flow set by the direction of the group velocity.

B. Linear dispersion with negative group velocity

If the dispersion is assumed to be linear but with $v_g < 0$, this reverses the sign of k_0 and one expects $\chi_{yy}(k, /) = \chi_{yy}(-k, \setminus)$. From Eq. (18) one can then show that

$$\tilde{S}_{21f}^{yy}(\omega, r, \setminus) = \tilde{S}_{21f}^{yy}(\omega, -r, /). \quad (27)$$

This is in line with the intuitive expectation that changing the sign of the group velocity (i.e., the direction in which energy propagates) is equivalent to exchanging the positions of the antenna emitting the power and that collecting the power. When $v_g < 0$, the energy flow is still unidirectional but now toward the $r < w$ half space.

VI. LEMMA TO EVALUATE THE RESPONSE TO SINGLE-SIDED WAVE-VECTOR SPACES

A. Splitting the full response into partial integrals

Since the dispersion relations and/or the rf fields are generally different for positive and negative wave vectors, it is interesting to split the full transmission response of Eq. (18) into a sum of two partial responses,

$$\tilde{S}_{21f} = \tilde{S}_{21+} + \tilde{S}_{21-}, \quad (28)$$

each accounting for half of the wave-vector space. Writing $I(\omega, k) = [\bar{h}^* \cdot [\bar{\chi}_{(\omega_0 + v_g k)} \cdot \bar{h}]] (h_u^{\text{rf}}(k))^2$ within the integrand of Eq. (18), we define the partial responses as $\tilde{S}_{21+}(\omega, r) = \int_0^{+\infty} I(\omega, k) e^{-ikr} dk$ and $\tilde{S}_{21-}(\omega, r) = \int_{-\infty}^0 I(\omega, k) e^{-ikr} dk$. They can be rewritten as

$$\tilde{S}_{21\pm}(\omega, r) = \int_{-\infty}^{+\infty} e^{-ikr} I(\omega, k) \Theta(\pm k) dk, \quad (29)$$

where $\Theta(k)$ is the Heaviside function.

B. Lemma

Using the inverse Fourier transform of the Heaviside function [43], we get

$$\begin{aligned} \tilde{S}_{21\pm}(\omega, r) &= \tilde{S}_{21f}(\omega, r) \otimes \left(\frac{1}{2} \delta(r) \mp \frac{i}{2\pi r} \right) \\ &= \frac{1}{2} \left(\tilde{S}_{21f}(\omega, r) \mp i\mathcal{HT}\{\tilde{S}_{21f}(\omega, r)\} \right), \end{aligned} \quad (30)$$

where δ is the Dirac function, \otimes indicates the convolution product, and the Hilbert transform \mathcal{HT} applies to the variable r .

By construction, the full response \tilde{S}_{21f} is the sum of the partial responses [Eq. (28)]. Interestingly, the lemma in Eq. (30) indicates that the full response can also be used to calculate the partial responses \tilde{S}_{21+} and \tilde{S}_{21-} . We will extensively use this trick later to combine full responses in computable cases (like for a line-shaped dispersion), in order to account for transmission responses in situations where spin waves possess nontrivial dispersion relations (like any broken-linear dispersion relation as in the V-shaped cases).

C. Physical meaning of the lemma: Envelope, modulation and Bedrosian theorem

The lemma in Eq. (30) indicates that, if the $k < 0$ branch was missing from the spectrum, the spatial dependence of $\tilde{S}_{21+}(\omega, r)$ would be a space-distorted version of the full response $\tilde{S}_{21f}(\omega, r)$, the distortion being due to the existence of the $-i\mathcal{HT}$ additional term.

We will see that, in the situations when $(\omega - \omega_0)/v_g = k_0 \gg \{1/L_{\text{att}}, 1/w\}$, the $\tilde{S}_{21f}(r)$ spectrum contains a *fast* modulation with a spatial period $2\pi/k_0$ embedded in a *slow* spatial envelope related to the spin-wave decay length L_{att} and the antenna efficiency function [see, e.g., Eq. (20)]. The real and imaginary parts of $\tilde{S}_{21f}(r)$ are in quadrature in these representative situations.

The (slow) envelope and the (fast) modulation may have almost disjointed supports in reciprocal space, such that the shape of the term $\mathcal{HT}\{\tilde{S}_{21f}(r)\}$ can be anticipated using the Bedrosian theorem. The transform $\mathcal{HT}\{\tilde{S}_{21f}(r)\}$ will be a signal embedded in the same, almost unaltered, (slow) envelope but the (fast) modulation will be translated in space by a quadrature displacement of length $\pi/(2k_0)$. Owing to the properties of the Hilbert transform, the sign of this displacement will depend on $\text{sgn}(r)$.

The distortion induced by the \mathcal{HT} terms within the partial integral changes the repartition of the signal between the two $r \in \mathbb{R}^+$ and $r \in \mathbb{R}^-$ half spaces. This is of premium importance when analyzing the nonreciprocity of spin-wave transmission from one antenna to the other and vice versa. We shall illustrate this point later with several dedicated examples.

VII. CASE OF V-SHAPED DISPERSION WITH DIAGONAL SUSCEPTIBILITY

Let us now analyze the case of spin waves possessing a V-shaped dispersion relation. We still consider $p = s = 0$ and an excitation by a diagonal susceptibility term only. In the relevant wave-vector interval, we write $\omega = \omega_0 + v_{g+}k$ for $k > 0$ and $\omega = \omega_0 + v_{g-}k$ for $k < 0$, with $v_{g+} > 0$ and $v_{g-} < 0$. At $\omega > \omega_0$, there are now two resonant wave vectors $k_{0+} > 0$ and $k_{0-} < 0$.

Because of the irregular (nondifferentiable) character of a V-shaped dispersion relation in $k = 0$, Eq. (21) describing the susceptibility is applicable only for $\omega \gtrsim \omega_0 + \Delta\omega_0$ when the spin waves are far above the gap ω_0 ; in the gap, the spin waves are evanescent. This situation will not be studied.

A. General case: Nonsymmetric V-shaped dispersion relation

In the general case when $-v_{g-} \neq v_{g+}$, the full response can then be expressed as

$$\tilde{S}_{21f}^{yy}(\omega > \omega_0, r, \vee) = \tilde{S}_{21-}^{yy}(\backslash, v_{g-}) + \tilde{S}_{21+}^{yy}(/, v_{g+}), \quad (31)$$

where each partial term is now evaluated with its own group velocity. The partial contributions of the $k < 0$ and $k > 0$ branches can be calculated using the lemma in Eq. (30):

$$\begin{aligned} \tilde{S}_{21f}^{yy}(\omega > \omega_0, \vee) &= \frac{1}{2} \left(\tilde{S}_{21f}^{yy}(\backslash, v_{g-}) + \tilde{S}_{21f}^{yy}(/, v_{g+}) \right) \\ &\quad + i\frac{1}{2}\mathcal{HT}\{\tilde{S}_{21f}^{yy}(\backslash, v_{g-}) - \tilde{S}_{21f}^{yy}(/, v_{g+})\}. \end{aligned} \quad (32)$$

The second line of the previous expression cannot be made explicit in a reasonably compact form in the general case.

B. Symmetric V-shaped dispersion relation

However, the situation simplifies when the dispersion relation is symmetric with $v_{g+} = -v_{g-} = v_g > 0$ and when the susceptibility is even in k with $\bar{\chi}(k) = \bar{\chi}(-k)$. In this case we define $L_{\text{att}} > 0$ and have

$$\begin{aligned} \tilde{S}_{21f}^{yy}(\omega > \omega_0, r, \vee) &= \frac{1}{2} \left(\tilde{S}_{21f}^{yy}(\omega, r, /, |v_g|) + \tilde{S}_{21f}^{yy}(\omega, -r, /, |v_g|) \right) \\ &\quad + i\frac{1}{2}\mathcal{HT}\{\tilde{S}_{21f}^{yy}(\omega, -r, /, v_g) - \tilde{S}_{21f}^{yy}(\omega, r, /, v_g)\}. \end{aligned} \quad (33)$$

1. Perfect reciprocity

Remembering that \mathcal{HT} transforms odd functions into even functions, we can see that

$$\tilde{S}_{21f}^{yy}(r, \vee) = \tilde{S}_{21f}^{yy}(-r, \vee). \quad (34)$$

While, for a line-shaped dispersion relation, the energy was propagating in a half space only, a V-shaped dispersion relation leads to a propagation of energy in the *whole* space, symmetrically with respect to the antenna center. (Note that, in this section, we consider a diagonal term of the susceptibility tensor.) In other words, a VNA-based

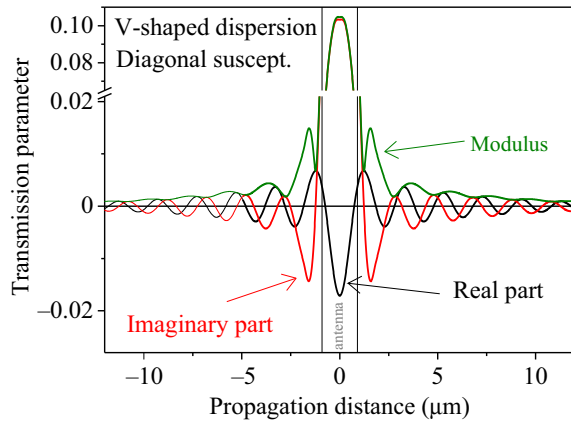


FIG. 8. Transmission parameter versus propagation distance in the case of a reciprocal, symmetric V-shaped dispersion relation when only one diagonal term of the susceptibility tensor is considered [Eq. (33)]. The attenuation length is $6 \mu\text{m}$. The two resonant wave vectors are $k_0 = \pm\pi \text{ rad}/\mu\text{m}$ corresponding to a spatial period of $2 \mu\text{m}$. The antenna width is $w = 1.8 \mu\text{m}$, with zero thickness ($p = 0$) and zero spacing ($s = 0$).

electrical measurement with *gedanken* antennas involving only the diagonal susceptibility terms would show a perfectly reciprocal behavior with $\tilde{S}_{21f}^{yy}(\nu) = \tilde{S}_{12f}^{yy}(\nu)$. This is illustrated in Fig. 8; the spatial dependence of $\tilde{S}_{21f}^{yy}(\nu)$ is plotted for typical experimental parameters.

2. Analytics

Above $\omega_0 + \Delta\omega_0$, the terms of Eq. (33) can be made explicit. The “direct” terms [the first term on the right-hand side of Eq. (33)] are straightforward to understand: they create the r -even equivalent of Eq. (22); i.e., the bidirectional (r -symmetrized) version of Fig. 7. They comprise propagating terms and local terms, in a manner similar to previously. These “direct” terms within $\tilde{S}_{21f}^{yy}(\omega > \omega_0, r, \nu)$ can be expressed as

$$\begin{aligned} & \frac{1}{2} \left(\tilde{S}_{21f}^{yy}(\omega, r, /, |v_g|) + \tilde{S}_{21f}^{yy}(\omega, -r, /, |v_g|) \right) \\ &= \underbrace{\sqrt{\frac{\pi}{2}} \mathcal{L}(\omega)}_{\text{Lorentzian}} \left[\underbrace{P_2(r+w, \omega) + P_2(r-w, \omega) - 2P_2(r, \omega)}_{\text{propagation terms}} \right. \\ & \quad \left. + \underbrace{\left(1 + \frac{iL_{\text{att}}(\omega - \omega_0)}{v_g} \right) (|r+w| + |r-w| - 2|r|)}_{\text{local terms}} \right], \end{aligned} \quad (35)$$

where the last line contains the local terms that depend on the positive-definite distances, and where the propagating

terms depend on the function

$$\begin{aligned} P_2(x, \omega) = & L_{\text{att}} e^{-|x|/L_{\text{att}}} \left[\Theta_{(x)} \exp\left(\frac{-ix(\omega - \omega_0)}{|v_g|}\right) \right. \\ & \left. + \Theta_{(-x)} \exp\left(\frac{ix(\omega - \omega_0)}{|v_g|}\right) \right]. \end{aligned} \quad (36)$$

The physical interpretation of Eq. (35) is straightforward: the local terms represent some autoinductance, and the propagating terms contain energy emitted by the center of the antenna and propagating to both its sides with the same decay length but opposite sense of phase rotation. They are complemented by other propagating terms for which the relevant travel distances are incremented or decremented by w , with the associated propagation loss and dephasing arising from the increment or decrement of the propagation distance.

The \mathcal{HT} -transformed term [the second term on the right-hand side of Eq. (33)] admits a very heavy analytical expression [see Appendix C, Eqs. (C1)–(C3)] for distant antennas (i.e., for $|r| > w$) [44]. The application of the expression is included in Fig. 8.

3. Dependence over propagation distance and frequency

From the Bedrosian theorem combined with the $\times i$ multiplication in the \mathbb{C} plane in the second term on the right-hand side of Eq. (33), one can anticipate that the “direct” term [first term on the right-hand side of Eq. (33)] and the Hilbert-transformed “indirect” term (second term on the right-hand side of that equation) have very similar shapes, except in the $|r| < w$ region where the signal is dominated by the local terms (not shown). For $|r| > w$, the phases of all terms within Eq. (33) rotate with the propagation distance and with the frequency at a pace essentially defined by the phase rotator functions $P_1(r, \omega)$ and $P_2(r, \omega)$. This is, for instance, clear in Fig. 8: the real and imaginary parts of the transmission signal change sign every time the propagation distance r is incremented by a half period, $\lambda/2 = \pi v_g/(\omega - \omega_0)$, of the spin wave. Equivalently, they change sign every time the frequency is incremented by $v_g/(2r)$.

Note that, while a mixture of Eqs. (20) and (36) is routinely used [4,7,19,21,42] to interpret propagating-spin-wave spectroscopy experiments by simply setting $x = r$, we emphasize that it is not always appropriate. Such a fitting procedure indeed confuses the propagating terms $P_2(r-w)$ and $P_2(r+w)$ with $P_2(r)$. This is valid as long as (i) one restricts to situations where $|r| \gg w$ (i.e., distant antennas) and (ii) one can neglect the contribution of the nondiagonal terms of the susceptibility tensor.

VIII. RESPONSE TO THE FULL SUSCEPTIBILITY TENSOR

So far we have looked at the consequence of the sole diagonal terms of the susceptibility tensor. This is over: from now on we take into account the complexity of \bar{h} that arises from its z component that is $\propto \text{sgn}(k)$ [see Eq. (17)]. This means that, from now on, helicity mismatch is included.

A. Accounting for the helicity dependence at emission and detection

The factor $[\bar{h}^* \cdot [\bar{\chi}(\omega, k) \cdot \bar{h}]]$ within the integrand of Eq. (18) contains two kinds of terms.

1. Regular susceptibility terms

The diagonal terms involving $\chi_{xx,yy,zz}$ as well as $\chi_{xy,yx}$ (which happen to vanish when the applied field is along x , as in all the situations studied hereafter) do not depend on the sign of k . For all these terms, the models with the yy superscript are applicable provided the proper χ_{\max} are used. The summation of Eq. (28) still holds:

$$\tilde{S}_{21f}^{yy}(\omega, r) = \tilde{S}_{21+}^{yy}(\omega, r) + \tilde{S}_{21-}^{yy}(\omega, r)$$

provided yy is replaced by the considered susceptibility term among $\{xx, yy, zz, xy, yx\}$.

2. Nondiagonal susceptibility terms involving \bar{h}_z exactly once

In contrast, the $1z$ terms involving χ_{yz} or χ_{zy} (as well as $\chi_{xz,xz}$, which happen to vanish when the applied field is along x , as in all the situations studied hereafter) involve \bar{h}_z exactly once; they are hence $\propto \text{sgn}(k)$, such that the partial integrals for the $k < 0$ and $k > 0$ branches must be calculated separately using the lemma in Eq. (30). For these terms, the combination of $\bar{h}_z \propto \text{sgn}(k)$ and Eq. (28) results in

$$\tilde{S}_{21f}^{1z}(\omega, r) = \tilde{S}_{21+}^{1z}(\omega, r) - \tilde{S}_{21-}^{1z}(\omega, r). \quad (37)$$

Using the lemma in Eq. (30), we get

$$\tilde{S}_{21f}^{1z}(\omega, r) = -i\mathcal{HT}\{\tilde{S}_{21f}^{yy}(\omega, r)\}, \quad (38)$$

where χ_{\max} on the right-hand side of the equation should be replaced by either χ_{yz}^{\max} or χ_{zy}^{\max} depending on the term being calculated. Note that χ_{yz}^{\max} and χ_{zy}^{\max} are opposite and real-valued at the resonance. We will see that in many situations Eq. (38) admits an analytical solution. Two points are worth mentioning: they concern the frequency content and the spatial content of Eq. (38).

(i) The Hilbert transform applies to the space variable r only. At a propagation distance r_0 , the frequency dependence of $\tilde{S}_{21f}^{1z}(r_0)$ will thus *always be the same* as $\tilde{S}_{21f}^{yy}(r_0)$.

Because of this appearance similarity, they cannot be distinguished by a frequency scan at a single propagation distance.

(ii) The spatial content of Eq. (38): once again, if sufficiently far from the resonance, i.e., if $|\omega - \omega_0| \gg \Delta\omega_0$, the Bedrosian theorem and the form of $\bar{\chi}$ indicate that the spatial variations of $\tilde{S}_{21f}^{1z}(\omega, r)$ versus $\tilde{S}_{21f}^{xx,yy,zz}$ may look like scaled complex conjugates. We will show later examples illustrating this point.

B. Full response in the most general case

The full response is the sum involving all terms of $\bar{\chi}$:

$$\tilde{S}_{21f} = \sum_{xx,yy,zz,xy,yx} \tilde{S}_{21f}^{yy} + \sum_{yz,zy,xz,zx} \tilde{S}_{21f}^{1z}.$$

We remind the reader that the static field is along the in-plane direction x .

The simplest case is when the total moment of the magnetic system has a longitudinal-only susceptibility (i.e., when $\bar{\chi}$ reduces to a sole vanishing term, which is χ_{xx}). This is, for instance, the case for the total moment of the optical mode of an SAF in the scissors state. In this case the full response reads simply

$$\tilde{S}_{21f}(\text{longitudinal } \bar{\chi}) = \tilde{S}_{21f}^{xx}, \quad \text{with } \chi_{\max} \in i\mathbb{R}^-, \quad (39)$$

such that the previous methodology can be used in a straightforward manner.

A more standard situation is when both diagonal and nondiagonal susceptibility terms that are transverse to the field are involved in the dynamics. This is, for instance, the case for the spin waves of in-plane-magnetized single layers above saturation, or for the total moment of the acoustic mode of an SAF. In these cases, we can use Eq. (38) and gather the terms as follows:

$$\tilde{S}_{21f}(\text{transverse } \bar{\chi}) = \underbrace{\sum_{yy,zz} \tilde{S}_{21f}^{yy}}_{\chi_{\max} \in i\mathbb{R}^-} - i\mathcal{HT} \left\{ \underbrace{\sum_{yz,zy} \tilde{S}_{21f}^{yy}}_{\chi_{\max} \in \mathbb{R}} \right\}. \quad (40)$$

(i) The first brace involves the two susceptibility terms that are Lorentzian, with a negative imaginary value χ_{\max} at the resonance. They lead to contributions $\propto S_{21f}^{yy}$, where the proportionality is a real number. These contributions resemble that of Fig. 6 or that of Fig. 8, depending on the shape of the dispersion relation.

(ii) The second brace involve susceptibility terms that have a real value $\mp i\epsilon \chi_{\max}$ at the resonance [see Eq. (8)]. As a result, the real parts of $\pm S_{21f}^{zy,yz}$ thus contribute to the imaginary part of the signal enclosed in curly brackets, and

the imaginary parts of $\pm S_{21f}^{yz,zy}$ contribute to the real part of the signal enclosed in curly brackets.

Beside, this signal is Hilbert-transformed according to the space variable r and then multiplied by $-i$. This process affects the spatial profile of the response, notably because the \mathcal{HT} transforms even functions in odd ones. However, situations may stay simple when the Bedrosian theorem is applicable, as detailed in a few examples below.

IX. RESPONSES INCLUDING THE NONDIAGONAL PARTS OF THE SUSCEPTIBILITY

A. Line-shaped dispersion: quasi-unidirectional energy flow

Let us consider the case of $\tilde{S}_{21f}(\omega, r, /)$, i.e., the total response including the whole susceptibility tensor for a dispersion relation that is line-shaped in the range of wave vectors allowed by the antenna. This situation mimics the spin waves within, for instance, an SAF in the scissors state with $\vec{k} \parallel \vec{H}$ (see Ref. [27]) or within a dipolarly coupled bilayer [see, for instance, Fig. 4(f) in Ref. [9]]. For a line-shaped dispersion relation, Eq. (38) can unfortunately not be simplified and has to be integrated numerically.

An example of a full signal and its contributing terms $\tilde{S}_{21f}^{yy}(/)$ and $\tilde{S}_{21f}^{1z}(/)$ is given in Fig. 9. The last panel compares the unidirectional case $\tilde{S}_{21f}^{yy}(\omega, r, /)$ obtained formerly for a diagonal susceptibility with the total response including all terms of the susceptibility tensor, a real antenna, and a representative ellipticity of the precession.

While the $S_{21f}^{yy}(/)$ term was perfectly unidirectional [i.e., strictly vanishing for $r \leq -w$; see Fig. 9(a)], the presence of the $1z$ terms makes the total response no longer single-sided; the $-i\mathcal{HT}$ terms in Eq. (40) add a signal that leaks into the $r \leq -w$ half space. The amplitude of this leak is tiny except when $\omega \approx \omega_0$ where the Bedrosian theorem is inadequate [45]. The unidirectional emission of the full signals $\tilde{S}_{21f}(/)$ or $\tilde{S}_{21f}(\backslash)$ is essentially maintained despite the $-i\mathcal{HT}$ terms. This quasi-unidirectional emission, already evidenced experimentally in Ref. [27], is of strong interest for applications.

B. Symmetric V-shaped dispersion: Amplitude nonreciprocity

Let us see what happens for a symmetric V-shaped dispersion relation. This represents, for instance, the case of the moment of a single-layer film above saturation in the Damon-Eshbach geometry. This can also represent the total moment of the acoustic mode of an SAF for $k \perp H_{dc}$. For a V-shaped dispersion relation, we have shown that

$$\tilde{S}_{21f}^{yy}(r, \vee) = \tilde{S}_{21f}^{yy}(-r, \vee).$$

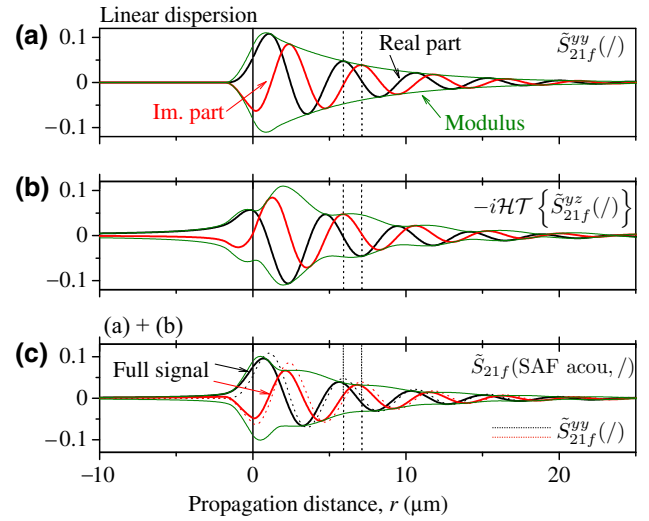


FIG. 9. Comparison of the two categories of terms contributing the antenna-to-antenna transmission parameter versus propagation distance for a linear dispersion relation [Eq. (40)]. The parameters are $p = s = 0$, $w = 1.8 \mu\text{m}$, $\omega_0 = 5 \text{ Grad/s}$, $\omega = 13 \text{ Grad/s}$, $L_{\text{att}} = 6 \mu\text{m}$, and $v_g = 6 \text{ km/s}$. (a) Appearance of a diagonal term: $\tilde{S}_{21f}^{yy}(/)$ for $\chi_{\text{max}} = -i$ i.e., corresponding to χ_{yy} . (b) Appearance of a $1z$ term: $-i\mathcal{HT}\{\tilde{S}_{21f}^{yy}(/)\}$ for $\chi_{\text{max}} = 1$. In practice the amplitude of this term will be decremented by the ellipticity factor ϵ . (c) Sum of (b) and (c) for $\epsilon/\sin(\varphi) = 0.3$, accounting for the full response of the acoustic spin-wave branch of an SAF with a linear dispersion relation according to Eq. (40). The vertical dotted lines are guides to the eye meant to evidence the evolution of the phase of the signal upon the $-i\mathcal{HT}\{\times i\}$ operation.

This r -even character expresses the fact that the yy terms lead to transmission signals that are free of amplitude nonreciprocity.

However, owing to the properties of the Hilbert transform, the terms below the second brace in Eq. (40) will thus be r -odd:

$$\tilde{S}_{21f}^{1z}(r, \vee) = -\tilde{S}_{21f}^{1z}(-r, \vee),$$

so that they add or subtract from the contribution of the diagonal terms of the susceptibility tensor, depending on the sign of r .

This leads to a self-evident statement: the r -even contributions $\tilde{S}_{21f}^{yy}(r, \vee)$ and r -odd contributions $\tilde{S}_{21f}^{1z}(r, \vee)$ can be separated easily in an experimental measurement in the V situation, by simply calculating $S_{21} + S_{12}$ or $S_{21} - S_{12}$. Using $\{\mathcal{HT}\}^2 = -1 \times$, Eq. (38), and Eq. (33), we can express $\tilde{S}_{21f}^{1z}(\omega, r, \vee)$ for $|r| \geq w$ as

$$\begin{aligned} \tilde{S}_{21f}^{1z}(r, \vee) = & -\frac{i}{2} \left(\tilde{S}_{21f}^{yy}(-r, /) - \tilde{S}_{21f}^{yy}(r, /) \right) \\ & - \frac{i}{2} \mathcal{HT} \{ \tilde{S}_{21f}^{yy}(r, /) + \tilde{S}_{21f}^{yy}(-r, /) \}, \quad (41) \end{aligned}$$

in which one should pay attention to use the χ_{\max} of the nondiagonal susceptibility term being considered. Only the first term can be made explicit. The second term of Eq. (41) must be integrated numerically.

As a last comment, let us mention that, in practice, the amplitude nonreciprocity is often measured by looking at the experimental quantity $S_{21}/S_{12}(r)$, which is

$$\frac{\tilde{S}_{21f}(\omega, r)}{\tilde{S}_{21f}(\omega, -r)}(\vee) = \frac{\sum_{yy \text{ terms}} \tilde{S}_{21f}^{yy}(r) + \sum_{1z \text{ terms}} \tilde{S}_{21f}^{1z}(r)}{\sum_{yy \text{ terms}} \tilde{S}_{21f}^{yy}(r) - \sum_{1z \text{ terms}} \tilde{S}_{21f}^{1z}(r)}, \quad (42)$$

where we have omitted the \vee labels. This corresponds to the commonly observed ‘‘amplitude nonreciprocity’’ of Damon-Eshbach modes [14] arising from helicity match or mismatch. Note that the terminology ‘‘amplitude nonreciprocity’’ is somewhat improper. Indeed, as soon as the nondiagonal susceptibility terms contribute to the transmission signal, the experimental quantity S_{21}/S_{12} is then neither real nor constant: it is both position-dependent and frequency-dependent.

X. DISCUSSION

A. Perfect helicity mismatch and its perception in the spectral response

An intriguing question to understand is why the concept of the angle for perfect helicity mismatch [Eq. (9), or, equivalently, the angle for no inductive detection, Eq. (14)] seems to have been missed or ignored so far; this is intriguing since it is a rather trivial consequence of the form of the susceptibility tensor [Eq. (8)] and the form of the rf field of an antenna [Eq. (17)].

The likely reason is that the HMM effect has no perceivable consequence in most of the situations encountered in previous works, in particular for single-layer films above saturation. Indeed, in the popular Damon-Eshbach configuration in single layers with or without Dzyaloshinskii interaction [46,47], one uses field orientations of $\varphi = \pm\pi/2$ far from the HMM angles, such that the HMM effect is irrelevant there.

In contrast, the much less studied backward volume configuration of spin waves in single layers corresponds to $\varphi = 0$ or π , which is much closer to φ_{HMM} . For $\varphi = 0$, the backward volume spin waves feature a \wedge -shaped dispersion relation, with an extremely small group velocity and an almost flat dispersion relation, rendering difficult propagating-spin-wave spectroscopy experiments [48–50]. For a single-layer film, as soon as the field is slightly tilted away from the backward volume configuration (in particular, when $\varphi = \varphi_{\text{HMM}}$), the spin waves recover a V-shaped dispersion relation with a forward character. When measuring $\tilde{S}_{21f}(r > 0)$, one looks at the energy transmission from antenna 1 to antenna 2, hence essentially only due

to the $k > 0$ spin waves that have a group velocity in the $1 \rightarrow 2$ direction. The main (propagating) part of the signal is thus provided by the term $\frac{1}{2}\tilde{S}_{21+}(r > 0, v_g^+)$ in Eq. (33). For this field orientation, the HMM direction is in the $k < 0$ side (or equivalently it is in the $\varphi_{\text{HMM}} + \pi$ orientation): this means that the spin waves that are not excited because of the perfect helicity mismatch would anyway not send energy in the direction to which one is sensitive; the spin waves able to transfer energy between antennas are not subjected to the HMM effect. It is therefore understandable that the concept of perfect helicity mismatch has been missed in earlier studies.

B. Applicability of the analytical approximations

A second important question is the range of applicability of the analytical approximations done after Eq. (18). The main approximation is the linearization of $\chi(k)$ [Eq. (21)] done for nonflat dispersion relations. While in the case of a line-shaped dispersion (Sec. V) this approximation is always legitimate, it is not near the singular point $\omega = \omega_0$ for broken-linear dispersion relations, and in particular for a V-shaped dispersion relation (Sec. VII). This pathological change of slope of $\omega(k)$ at $k = 0$ happens every time an *infinitely* extended magnetic system is considered. This singularity at the dispersion relation $k = 0$ is not so much of a problem in practice because real antennas are unable to generate at strictly $k = 0$ (see note [33]).

Besides, any real magnetic system has a finite lateral size L , so that this singularity disappears: the dispersion relation becomes regular (differentiable) at $k = 0$ and the frequency ω_0 changes slightly because of the shape anisotropy associated with the finite dimension. We can thus model the $|k| < 1/L$ part of the spectrum within the flat band model, which yields a substantial response only within the space very near to the emitter antenna (see Fig. 12).

If, in contrast, one excites the system at larger k , i.e., ‘‘far’’ [51] ferromagnetic resonance (FMR), the $k = 0$ singularity of the dispersion relation becomes irrelevant and we expect a response like that of Fig. 8 made unsymmetrical by the distortion of Eq. (42). In between these two frequency domains, an intermediate behavior should be found, in which the travelling character of the spin waves gets progressively perceivable in the r dependence of $\tilde{S}_{21f}(\vee)$.

C. On the deduction of dispersion relation from transmission spectra

Propagating-spin-wave spectroscopy (PSWS) is usually conducted to get information about the dispersion relation of spin waves or, at least, their group velocities. The zero-damping limit [Eq. (20)] can be used to qualitatively interpret PSWS experiments. For a more quantitative analysis, one typically [7,19,42] adds a propagation loss term

and uses the ansatz [21]

$$\tilde{S}_{21}^{\text{single mode}}(k(\omega)) \propto ie^{-ik|r|} e^{-|r|/L_{\text{att}}} (h_u^{\text{rf}}(k))^2. \quad (43)$$

We emphasize that it is not always appropriate. First, because generally several families of spin waves coexist in the spin-wave conduit so that the phase of the transmission coefficient at a given frequency is influenced by more than one single k value. This first problem can sometimes be circumvented if an appropriate group-velocity-selective method is used to isolate the contribution of a family of spin waves [4]. However, the use of Eq. (43) confuses the propagating terms $P_2(r-w)$ and $P_2(r+w)$ with $P_2(r)$ in Eq. (36), which is only valid when $|r| \gg w$ (i.e., distant antennas). Besides, the use of Eq. (43) is equivalent to neglecting the contribution of the nondiagonal terms of the susceptibility tensor, such that the part of the spectrum influenced by the vicinity of $k=0$ is not modeled correctly. As a reminder, care should be taken when using Eq. (43) to quantitatively model entire transmission spectra.

As a result, the recording of solely frequency-resolved transmission spectra is generally not sufficient to deduce the dispersion relation. When trying to get $\omega(k)$ from an experimental spectrum, one faces an additional difficulty: the phase $-ikr$ in PSWS data is known only modulo 2π . A starting point along the dispersion relation is thus needed to deduce the whole dispersion relation. One generally uses the value of $\omega(k=0)$ which—in contrast to common thinking—cannot be extracted from the PSWS data alone. Indeed, the frequency-resolved transmission spectra have qualitatively similar shapes (envelope and oscillations therein) for V-shaped and line-shaped dispersion relations [52] but the frequency $\omega(k=0)$ can be at various positions within the envelope, depending on the type of dispersion relation and the shape of the antenna (single-wire as in Fig. 1, U-shaped as in [7], etc.).

For instance, the $\omega(k=0)$ frequency is $\Delta\omega_0 \neq 0$ above the onset of the envelope for a V-shaped dispersion relation (devices with a single-wire antenna harnessing Damon-Eshbach magnetostatic spin waves [19] or forward volume spin waves). The $\omega(k=0)$ frequency is $\Delta\omega_0 \neq 0$ below the roll-off of the envelope for devices with a single-wire antenna and \wedge -shaped dispersion relation (backward volume spin waves). It is the middle of the envelope for devices with a single-wire antenna and line-shaped dispersion relation (Fig. 6). In all other cases (more complex form of dispersion relation and/or antenna emitting a spectrum that is not maximal at $k=0$), the $\omega(k=0)$ frequency can be anywhere within (or without) the envelope and therefore cannot be identified from knowledge of a PSWS spectrum alone. For good practice, the $\omega(k=0)$ frequency ought to be measured separately, optimally by classical FMR.

XI. ONE-WAY FILTERS THAT ARE TUNABLE BETWEEN LOW-PASS, ALL-PASS, AND HIGH-PASS

When using spin waves for signal or information processing in nanodevices, the main engineering issue is the overall energy efficiency. Solutions have been developed to focus the spin-wave energy [53,54] at a particular position. Solutions have also been found to compensate for the propagation loss of spin-wave energy [55]. However, the bottleneck remains the low power efficiency at transduction back and forth from the electrical domain to the spin-wave domain: a gain between one and two orders of magnitude is required. Ensuring a unidirectional energy flow of the spin-wave energy is a step in the right direction because this avoids wasting half of the energy that the spin waves would be otherwise radiating in the unwanted direction.

A. Combining single-sided k emission with unidirectional energy flow

Besides, the unidirectional energy flow can be combined with the single-sided k emission to design one-way reconfigurable frequency filters. Let us illustrate this assuming the quasi-line-shaped dispersion relation of an SAF with $\vec{k} \parallel \vec{H}_{x,\text{dc}}$, which offers $\text{sgn}(v_g^+) \approx \text{sgn}(v_g^-)$, the two being, for instance, negative to ensure a unidirectional energy flow from antenna 2 to antenna 1 [see the example of Fig. 10(a)]. Indeed, in this situation, the transmission $\tilde{S}_{21f}(r > 0)$ above ω_0 is due to the $k < 0$ branch, while the transmission below ω_0 is due to the $k > 0$ branch. The sum of the two partial contributions leads to a transmission spectrum that extends symmetrically around the uniform resonance ω_0 , as was the case in Fig. 6. We can name this behavior “all-pass,” and it can be obtained for the total moment of the acoustic SW mode of an SAF with $\vec{k} \parallel \vec{H}_x$, i.e., $\varphi = 0$, as demonstrated experimentally in Ref. [27].

For the acoustic mode of an SAF, slightly turning the applied field from $\varphi = 0$ to $\varphi = \varphi_{\text{HMM}}$ maintains [27] the property $\text{sgn}(v_g^+) = \text{sgn}(v_g^-)$: the dispersion relation is broken-linear but still monotonic across $k=0$. Since $v_g^+ \neq v_g^-$, none of the analytical limits described above apply, and a numerical integration of Eq. (18) must be performed. For this new field orientation φ_{HMM} , the perfect helicity mismatch cancels the contribution from the $k < 0$ branch, such that the transmission is almost entirely suppressed above ω_0 . This “low-pass” filtering can be changed to “high-pass” filtering by rotating the dc field in the opposite direction. Examples of these “all-pass,” “low-pass,” and “high-pass” behaviors are shown in Fig. 10. Note that the frequency filtering is obtained while maintaining a unidirectional energy transfer, similar to that of Fig. 9.

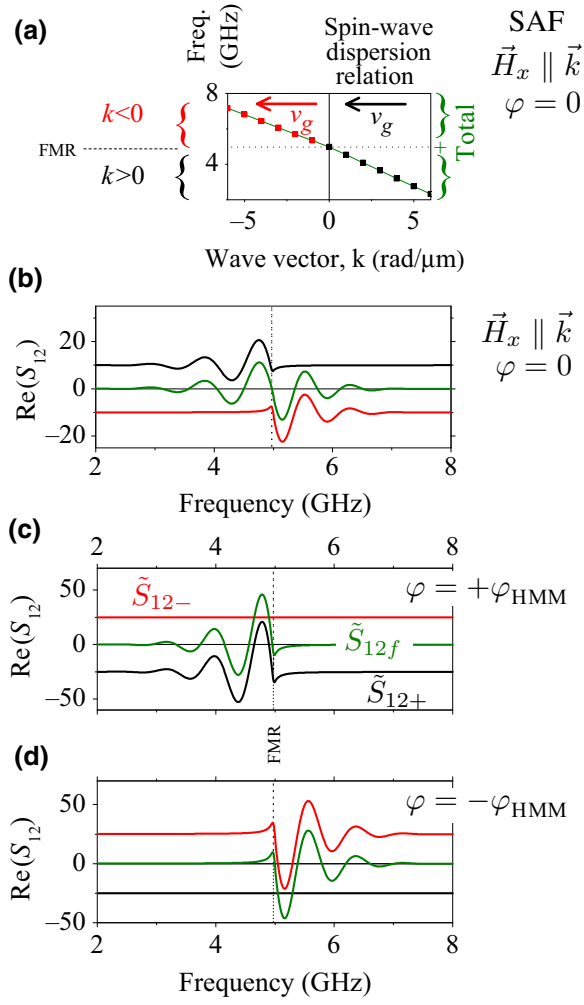


FIG. 10. Illustration of the combination of single-sided k emission and unidirectional energy flow. (a) Linearized dispersion relation of the acoustic mode of a synthetic antiferromagnet for a wave vector parallel to the applied field ($\varphi = 0$), according to Ref. [27]. The material parameters are from Ref. [36] with $\alpha = 0.001$ and $\mu_0 H_x = 50$ mT. (b)–(d) Numerical evaluations [Eq. (18)] of the partial responses S_{12+} and S_{12-} and the full response S_{12f} for an antenna geometry with $r = 3 \mu\text{m}$, $w = 0.8 \mu\text{m}$, and $p = s = 0$. In panel (b), the dc field is oriented at $\varphi = 0$, such that only h_z^{eff} contributes. In panel (c), the dc field is tilted by -16° to achieve perfect helicity mismatch for the $k < 0$ branches, thereby achieving a “high-pass” behavior. The field rotation is opposite in panel (d). The dispersion relations for panels (c) and (d) are qualitatively similar to that for panel (a) and they are taken from Ref. [27].

B. Alternative materials for reconfigurable filtering

The previous proposition—one-way filters that are tunable between low-pass, all-pass, and high-pass—relies on two ingredients: a monotonic dispersion relation so that the frequencies of the $k < 0$ spin waves and $k > 0$ spin waves differ, and the ellipticity of the inductive response of the total moment of the magnetic system. While the

second ingredient is fairly easy to obtain, the first one has so far been demonstrated only at low k values in bilayers [9] and in SAFs [27]. Since it relies on the layer-to-layer dipolar interaction, monotonic dispersion relations should occur in many more magnetic systems that can be prepared in states that are analogues of the antiparallel state or of a scissors state. This task of searching for systems that can host unidirectional spin waves exceeds the scope of our present study. However, it would be interesting to investigate several systems in particular. This includes, for instance, bilayers in which the two layers are exchanged-biased in opposite directions. This includes also antiferromagnetically coupled multilayers (“multi-SAFs”), as well as simple multilayers that would comprise layers that possess a contrast of coercivity and/or anisotropy so that the multilayer can be prepared in nontrivial magnetic configurations.

XII. CONCLUSIONS

This paper extends the formalism of spectroscopy of propagating spin waves when using inductive antennas connected to a vector network analyzer. The problem is supposed to be invariant in the plane transverse to the spin-wave wave vector.

The paper first revisits an apparently simple problem: the magnetic field generated by a single-wire antenna and how it excites the magnetization precession. From a reciprocal-space analysis of the antenna field, we describe the phenomenon of helicity match or mismatch between the dynamic magnetization of a spin wave and the magnetic field radiated by the antenna. From the form of the susceptibility tensor reflecting the precession ellipticity, we identify specific orientations of the wave vector for which a perfect helicity mismatch is reached, such that the antenna cannot excite this spin wave, while it can for the opposite wave vector—this single-sided wave-vector generation is not to be confused with a unidirectional emission of energy.

We then analyze the stray field emanating from a spin wave, and how this stray field couples to an antenna used as an inductive detector. It appears that spin waves of properly chosen helicity do not emit any stray field on one side of the film. Inductive detection of these spin waves is impossible. These spin waves are also the ones leading to perfect helicity mismatch. In simple terms, if an antenna cannot excite a given spin wave, it cannot detect it inductively: they do not couple and are dark to each other.

In the second part of the paper, we combine emission, propagation, and detection of spin waves to issue a formalism to calculate the antenna-to-antenna transmission. This formalism is applied to situations that lead to physically transparent analytical expressions. These expressions clarify the distinct roles of the direction of the wave vector of the spin waves, and of the direction of their group velocity.

Three canonical situations are examined: when spin waves have a flat dispersion relation, a V-shaped dispersion relation, and finally a line-shaped dispersion relation. In the first case (vanishing group velocity), the spin waves radiate energy in a slightly nonreciprocal manner but in an only evanescent way. In contrast, for the very often encountered situation of a V-shaped dispersion relation, the emission of spin waves is bidirectional and comes with some nonreciprocity. This nonreciprocity is mainly of amplitude type, but varies with frequency and propagation distance.

For spin waves with a line-shaped dispersion relation in the range of wave vectors allowed by the antenna geometry, the spin waves transport power in a quasi-unidirectional manner. This happens for the acoustic spin waves of synthetic antiferromagnets when the spin-wave wave vector is close to parallel to the applied field. This situation is of interest for applications, and can be used to design filters that can be reconfigured to be low-pass, high-pass, or all-pass. The present formalism offers a simple and direct method to understand, design, and optimize devices harnessing propagating spin waves, including when a unidirectional energy flow is desired, and when a frequency-filtering behavior is targeted.

ACKNOWLEDGMENTS

I acknowledge the French National Research Agency (ANR) under Contract No. ANR-20-CE24-0025 (MAX-SAW). I thank the authors of Ref. [21] for discussion during the elaboration of earlier generations of the present model, and Claude Chappert for insightful comments.

APPENDIX A: FIELD RADIATED BY AN ANTENNA OF RECTANGULAR CROSS SECTION

The field radiated by a rectangular antenna of finite thickness p , finite width w , and placed at a spacing z from the film has two components (Fig. 1). The in-plane component H_u^{rf} is the sum of two terms. Defining $\Sigma = (1/(2\pi))(\mu_0 I^{\text{rf}}/w)$ as a scaling factor that has the dimension of a flux density, the first term reads

$$\Sigma \left(\frac{p+z}{z} \left[\tan^{-1} \left(\frac{\frac{1}{2}w+u}{p+z} \right) - \tan^{-1} \left(\frac{u-\frac{1}{2}w}{p+z} \right) \right] + \frac{z}{p} \left[\tan^{-1} \left(\frac{u-\frac{1}{2}w}{z} \right) - \tan^{-1} \left(\frac{\frac{1}{2}w+u}{z} \right) \right] \right). \quad (\text{A1})$$

The second term of H_u^{rf} is

$$\Sigma \left[\frac{\frac{1}{2}w-u}{2p} \ln \left(\frac{p^2+2pz}{(u-\frac{1}{2}w)^2+z^2} + 1 \right) + \frac{\frac{1}{2}w+u}{2p} \ln \left(\frac{p^2+2pz}{(\frac{1}{2}w+u)^2+z^2} + 1 \right) \right]. \quad (\text{A2})$$

The out-of-plane component H_z^{rf} is also the sum of two terms. The first is

$$\Sigma \left(\frac{(u-\frac{1}{2}w)}{p} \left[\tan^{-1} \left(\frac{p+z}{u-\frac{1}{2}w} \right) - \tan^{-1} \left(\frac{z}{u-\frac{1}{2}w} \right) \right] - \frac{(\frac{1}{2}w+u)}{p} \left[\tan^{-1} \left(\frac{p+z}{\frac{1}{2}w+u} \right) - \tan^{-1} \left(\frac{z}{\frac{1}{2}w+u} \right) \right] \right) \quad (\text{A3})$$

while the second term of H_z^{rf} is

$$\Sigma \left(\frac{p+z}{2h} \ln \frac{(u-\frac{1}{2}w)^2/(p+z)^2+1}{(\frac{1}{2}w+u)^2/(p+z)^2+1} + \frac{z}{2p} \ln \frac{(\frac{1}{2}w+u)^2/z^2+1}{(u-\frac{1}{2}w)^2/z^2+1} \right). \quad (\text{A4})$$

APPENDIX B: FLAT HORIZONTAL DISPERSION WITH DIAGONAL SUSCEPTIBILITY

Let us consider the hypothetical case when the spin waves would have a perfectly flat dispersion relation (i.e., with $\omega(k) = \omega_0$, for all k) such that no resonant k_0 can be defined. In this section, we assume a realistic antenna with a finite thickness (i.e., $p \neq 0$) and at a finite spacing from the film (i.e., $z \neq 0$). In the following sections (Appendixes B 1 and B 2), we start by considering that the magnet is excited by only a diagonal susceptibility term (this assumption will be removed in Appendix B 3). Under these assumptions, the frequency and spatial dependences of $\tilde{S}_{21f}^{\text{yy}}(-)$ become separable:

$$\tilde{S}_{21f}^{\text{yy}}(\omega, r, -) \propto [\bar{h}^* \cdot [\bar{\chi}(\omega_0) \cdot \bar{h}]] \int_{-\infty}^{\infty} dk e^{-ikr} (h_u^{\text{rf}}(k))^2 = \tilde{s}_{21}^{\text{yy}}(\omega_0) \times s_{21}^{\text{yy}}(r, -). \quad (\text{B1})$$

1. Frequency dependence for a flat dispersion and a diagonal susceptibility

The complex-valued frequency dependence $\tilde{s}_{21}^{\text{yy}}(\omega_0)$ is simply that of the considered diagonal element of $\bar{\chi}(\omega, k = 0)$, i.e., a Lorentzian response centered at ω_0 , exactly like in an FMR measurement.

2. Spatial dependence for a flat dispersion and a diagonal susceptibility

The distance dependence $s_{21}^{yy}(r)$ is a real-valued, even, positive function that depends only on the antenna geometry. It is the convolution of the inverse Fourier transforms of each of the three factors of the squared equation (6):

(i) the inverse Fourier transform of the sinc^2 factor, which is $(\sqrt{2\pi}/w)\Lambda(r/w)$, where $\Lambda(r)$ is the unit triangular function vanishing at $|r| \geq w$;

(ii) the inverse Fourier transform of $e^{-2|k|s}$, i.e., $(4/(\sqrt{2\pi}))s/(r^2 + 4s^2)$; and

(iii) the inverse Fourier transform of the finite-antenna-thickness factor $(1 - e^{-p|k|})/(p|k|)^2$, which can be expressed in terms of the function g defined as

$$\begin{aligned} \sqrt{2\pi} g\left(\frac{p}{r}\right) &= 2r \left(\tan^{-1}\left(\frac{2p}{r}\right) + 2 \tan^{-1}\left(\frac{r}{p}\right) - \pi \right) \\ &+ 4p \left(\coth^{-1}\left(\frac{3p}{p-2ir}\right) \right. \\ &\left. + \coth^{-1}\left(\frac{3p}{p+2ir}\right) \right). \end{aligned} \quad (\text{B2})$$

Overall, the spatial decay of the spin-wave signal is

$$s_{21}^{yy}(r, -) = (2\pi)^{-3/2} \underbrace{\left[\frac{4}{w} \Lambda\left(\frac{r}{w}\right) \right]}_{w\text{-dependent}} \otimes \underbrace{\left(\frac{s}{r^2 + 2s^2} \right)}_{s\text{-dependent}} \otimes \underbrace{g\left(\frac{p}{r}\right)}_{p\text{-dep.}}. \quad (\text{B3})$$

A (very heavy) analytical formulation of this spatial decay exists. However, the notation of Eq. (B3) is much more insightful since its three factors depend on different geometrical terms: the antenna width w , its spacing with the film s , and the antenna thickness p .

In the case of (very unpractical experimentally!) partial overlap between the emitting and the receiving antenna, i.e., for $|r| \leq w$, the spatial decay resembles $\Lambda(r/w)$, hence linearly decreasing with a zero intercept for $|r| = w$ (see Fig. 11).

The convolution with the Lorentzian function of width s , and the cusp-shaped function g that has a width related to the antenna thickness p , makes the function $s_{21}^{yy}(r, -)$ nonvanishing for $|r| \gg w$ (see Fig. 11, inset). If $|r| \gg w$ and $p = 0$, then one can show that

$$s_{21}^{yy}(r \rightarrow \pm\infty, -) \propto \frac{1}{r^2}.$$

This scaling can be understood as the consequence of the $1/r^2$ decay of the antenna in-plane field, as already noted in Ref. [21]. This long-range exciting field (directly) induces (unretarded) magnetization dynamics below the receiving

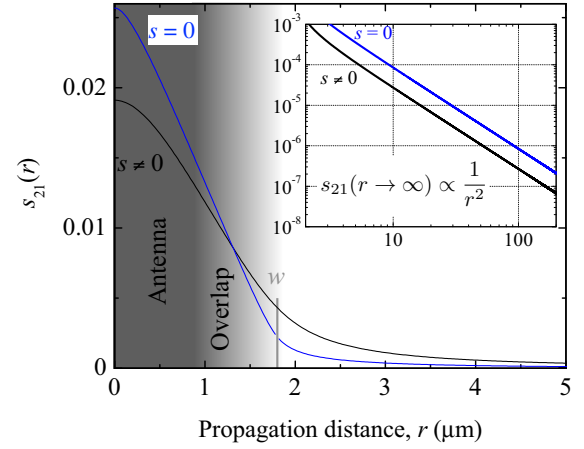


FIG. 11. Spatial decay $s_{12}^{yy}(r, -)$ for a flat dispersion relation and a response to the diagonal susceptibility terms only, according to Eq. (B3). Inset: likewise for large propagation distances. The antenna has a width $w = 1.8 \mu\text{m}$ and a thickness $p = 0.15 \mu\text{m}$.

antenna even if spin waves originating from the emitter antenna never travel there because of their vanishing ability to transport energy (i.e., $v_g = 0$). Note that other mechanisms—like antenna-to-antenna direct inductive coupling inducing current at the receiving antenna—also contribute to the distant excitation of quasi-uniform spin waves [56]. This second mechanism is ignored here but for both these scenarios the mutual inductance of the two antennas includes a contribution from the sample susceptibility at $k = 0$ that is detectable experimentally [4].

3. Spatial decay for a flat dispersion relation and all susceptibility terms

Finally, let us include the $1z$ terms in the full response when the dispersion relation is assumed flat.

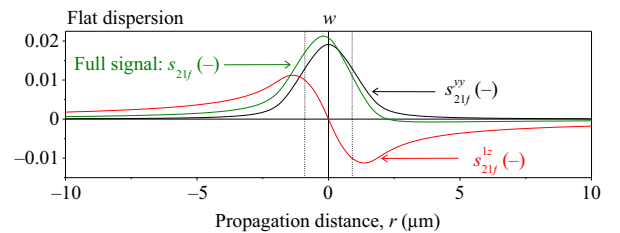


FIG. 12. Antenna-to-antenna transmission parameter versus propagation distance for a flat dispersion relation: the real-valued term s_{21}^{yy} [Eq. (B3)] normalized by $\chi_{\text{max}} = -i$, the real-valued term $-i\mathcal{HT}\{s_{21}^{1z}\}$ normalized by $\chi_{\text{max}} = 1$, and the full spatial decay $\tilde{S}_{21f}(\omega, r, -)/s_{21f}(\omega, r, -)$ when $\epsilon/\sin(\varphi) = 0.3$. The parameters are $p = s = 0.15 \mu\text{m}$ and $w = 1.8 \mu\text{m}$.

It reads

$$S_{21f}(\omega, r, -) = \tilde{s}_{21}(\omega) \times \left(\underbrace{\sum_{xx,yy,zz} s_{21}(r, -)}_{\chi_{\max} \in i\mathbb{R}^-} - i\mathcal{HT} \left\{ \underbrace{\sum_{yz,zy} s_{21}(r, -)}_{\chi_{\max} \in \mathbb{R}} \right\} \right), \quad (\text{B4})$$

where the proper χ_{\max} terms should be put in each term of the sums. Figure 12 illustrates how the two terms of Eq. (B4) depend on the propagation distance. Looking back at Fig. 2(a), we see that the quantities $s_{21f}^{yy}(-)$ and $s_{21f}^{zz}(-)$ look like smoothed versions of the real-space profile of the antenna fields h_u^{rf} and h_z^{rf} . The smoothing is essentially a convolution performed using the largest quantity among the antenna width, thickness, and spacing [see Eq. (B3)].

The frequency content of $\tilde{S}_{21f}(-)$ is still a Lorentzian function centered at ω_0 . However, the spatial content (Fig. 12) is no longer r -symmetric, since the \mathcal{HT} terms are r -odd. Somehow, even if the energy of the spin waves leaks in an only-evanescent way to the left and the right of the antenna, the helicity match or mismatch still results in a slightly stronger transmission $\tilde{S}_{21f}(r, -)$ toward the side of best helicity matching.

APPENDIX C: INDIRECT TERMS FOR A V-SHAPED DISPERSION RELATION AND A DIAGONAL SUSCEPTIBILITY TERM

Writing $E_1(v)$ for the exponential integral function of the complex numbers 1 and v , and G for the Meijer G function, the ‘‘indirect’’ term $+i\frac{1}{2}\mathcal{HT}\{\tilde{S}_{21f}^{yy}(\omega, -r, /, v_g) - \tilde{S}_{21f}^{zz}(\omega, r, /, v_g)\}$ [i.e., the second term on the right-hand side of Eq. (33)] is equal to the prefactor

$$\frac{i}{\sqrt{2\pi}} L_{\text{att}} \mathcal{L}(\omega) \exp\left(-\frac{2w+x}{L_{\text{att}}} - \frac{i(w(5\omega + \omega_0) + x(\omega + \omega_0))}{v_g}\right) e^{w/L_{\text{att}}} \quad (\text{C1})$$

multiplied by the sum of two terms, which are as follows. First term:

$$\begin{aligned} & -2 \exp\left\{w\left(\frac{1}{L_{\text{att}}} + \frac{i(5\omega + \omega_0)}{v_g}\right)\right\} \left(\exp\left\{\frac{2ix\omega_0}{v_g}\right\} E_1\left(-\frac{x(v_g + iL_{\text{att}}(\omega - \omega_0))}{L_{\text{att}}v_g}\right)\right. \\ & \left. + \exp\left\{2x\left(\frac{1}{L_{\text{att}}} + \frac{i\omega}{v_g}\right)\right\} E_1\left(x\left(\frac{i(\omega - \omega_0)}{v_g} + \frac{1}{L_{\text{att}}}\right)\right)\right) \\ & -2 \exp\left\{w\left(\frac{1}{L_{\text{att}}} + \frac{i(5\omega + \omega_0)}{v_g}\right)\right\} \left(-\ln\left(1 - \frac{w^2}{x^2}\right) \exp\left\{x\left(\frac{1}{L_{\text{att}}} + \frac{i(\omega + \omega_0)}{v_g}\right)\right\}\right) \\ & + \exp\left\{\frac{2x}{L_{\text{att}}} + \frac{2i(w(2\omega + \omega_0) + x\omega)}{v_g}\right\} E_1\left(-\frac{(w-x)(v_g + iL_{\text{att}}(\omega - \omega_0))}{L_{\text{att}}v_g}\right) \\ & - \exp\left\{\frac{2ix\omega_0}{v_g}\right\} \left(\exp\left\{\frac{2iw(2\omega + \omega_0)}{v_g}\right\} - 2 \exp\left\{w\left(\frac{1}{L_{\text{att}}} + \frac{i(5\omega + \omega_0)}{v_g}\right)\right\}\right) E_1\left(\frac{(w-x)(v_g + iL_{\text{att}}(\omega - \omega_0))}{L_{\text{att}}v_g}\right) \\ & + \exp\left\{\frac{2i(\omega_0(w+x) + 2w\omega)}{v_g}\right\} E_1\left(-\frac{(w+x)(v_g + iL_{\text{att}}(\omega - \omega_0))}{L_{\text{att}}v_g}\right) \\ & + \exp\left\{\frac{2(w+x)}{L_{\text{att}}} + \frac{2i\omega(3w+x)}{v_g}\right\} E_1\left(\frac{(w+x)(v_g + iL_{\text{att}}(\omega - \omega_0))}{L_{\text{att}}v_g}\right). \end{aligned} \quad (\text{C2})$$

Second term:

$$\begin{aligned} & -\pi \left(\exp\left\{-\frac{w}{L_{\text{att}}}\right\}\right) \left(\exp\left\{w\left(\frac{1}{L_{\text{att}}} + \frac{i\omega}{v_g}\right)\right\} - \exp\left\{\frac{iw\omega_0}{v_g}\right\}\right)^2 \exp\left\{\frac{x}{L_{\text{att}}} + \frac{i(w(3\omega + \omega_0) + x(\omega + \omega_0))}{v_g}\right\} \\ & \times G_{2,3}^{2,1}\left(-\frac{(w-x)(v_g + iL_{\text{att}}(\omega - \omega_0))}{L_{\text{att}}v_g} \middle| \begin{matrix} 0, -\frac{1}{2} \\ 0, 0, -\frac{1}{2} \end{matrix}\right). \end{aligned} \quad (\text{C3})$$

- [1] M. Bailleul, D. Olligs, and C. Fermon, Propagating spin wave spectroscopy in a permalloy film: A quantitative analysis, *Appl. Phys. Lett.* **83**, 972 (2003).
- [2] S. O. Demokritov, *Spin Wave Confinement: Propagating Waves*, 2nd edn. (Pan Stanford Publishing Pte. Ltd., Singapore, 2017), <https://www.crcpress.com/Spin-Wave-Confinement-Propagating-Waves-Second-Edition/Demokritov/p/book/9789814774352>.
- [3] V. Vlaminck and M. Bailleul, Current-induced spin-wave Doppler shift, *Science* **322**, 410 (2008).
- [4] T. Devolder, G. Talmelli, S. M. Ngom, F. Ciubotaru, C. Adelmann, and C. Chappert, Measuring the dispersion relations of spin wave bands using time-of-flight spectroscopy, *Phys. Rev. B* **103**, 214431 (2021).
- [5] A. V. Chumak, V. I. Vasyuchka, A. A. Serga, and B. Hillebrands, Magnon spintronics, *Nat. Phys.* **11**, 453 (2015).
- [6] G. Csaba, A. Papp, and W. Porod, Perspectives of using spin waves for computing and signal processing, *Phys. Lett. A* **381**, 1471 (2017).
- [7] G. Talmelli, T. Devolder, N. Träger, J. Förster, S. Wintz, M. Weigand, H. Stoll, M. Heyns, G. Schütz, I. P. Radu, J. Gräfe, F. Ciubotaru, and C. Adelmann, Reconfigurable submicrometer spin-wave majority gate with electrical transducers, *Sci. Adv.* **6**, eabb4042 (2020).
- [8] L. Körber, C. Heins, T. Hula, J.-V. Kim, S. Thlang, H. Schultheiss, J. Fassbender, and K. Schultheiss, Pattern recognition in reciprocal space with a magnon-scattering reservoir, *Nat. Commun.* **14**, 3954 (2023).
- [9] H. Qin, R. B. Holländer, L. Flajšman, F. Hermann, R. Dreyer, G. Woltersdorf, and S. van Dijken, Nanoscale magnonic Fabry-Pérot resonator for low-loss spin-wave manipulation, *Nat. Commun.* **12**, 2293 (2021).
- [10] O. Gladii, M. Collet, K. Garcia-Hernandez, C. Cheng, S. Xavier, P. Bortolotti, V. Cros, Y. Henry, J.-V. Kim, A. Anane, and M. Bailleul, Spin wave amplification using the spin Hall effect in permalloy/platinum bilayers, *Appl. Phys. Lett.* **108**, 202407 (2016).
- [11] L. Thevenard, C. Gourdon, J. Y. Prieur, H. J. von Bardeleben, S. Vincent, L. Becerra, L. Largeau, and J.-Y. Duquesne, Surface-acoustic-wave-driven ferromagnetic resonance in (Ga,Mn)(As,P) epilayers, *Phys. Rev. B* **90**, 094401 (2014).
- [12] G. Talmelli, F. Ciubotaru, K. Garello, X. Sun, M. Heyns, I. P. Radu, C. Adelmann, and T. Devolder, Spin-wave emission by spin-orbit-torque antennas, *Phys. Rev. Appl.* **10**, 044060 (2018).
- [13] V. F. Dmitriev and B. A. Kalinikos, Excitation of propagating magnetization waves by microstrip antennas, *Sov. Phys. J.* **31**, 875 (1988).
- [14] T. Schneider, A. A. Serga, T. Neumann, B. Hillebrands, and M. P. Kostylev, Phase reciprocity of spin-wave excitation by a microstrip antenna, *Phys. Rev. B* **77**, 214411 (2008).
- [15] D. D. Stancil, *Theory of Magnetostatic Waves* (Springer, New York, NY, 1993).
- [16] V. Vlaminck and M. Bailleul, Spin-wave transduction at the submicrometer scale: Experiment and modeling, *Phys. Rev. B* **81**, 014425 (2010).
- [17] V. E. Demidov, M. P. Kostylev, K. Rott, J. Münchberger, G. Reiss, and S. O. Demokritov, Excitation of short-wavelength spin waves in magnonic waveguides, *Appl. Phys. Lett.* **99**, 082507 (2011).
- [18] F. Vanderveken, V. Tyberkevych, G. Talmelli, B. Sorée, F. Ciubotaru, and C. Adelmann, Lumped circuit model for inductive antenna spin-wave transducers, *Sci. Rep.* **12**, 3796 (2022).
- [19] F. Ciubotaru, T. Devolder, M. Manfrini, C. Adelmann, and I. P. Radu, All electrical propagating spin wave spectroscopy with broadband wavevector capability, *Appl. Phys. Lett.* **109**, 012403 (2016).
- [20] T. Devolder, S.-M. Ngom, A. Mouhoub, J. Létang, J.-V. Kim, P. Crozat, J.-P. Adam, A. Solignac, and C. Chappert, Measuring a population of spin waves from the electrical noise of an inductively coupled antenna, *Phys. Rev. B* **105**, 214404 (2022).
- [21] M. Sushruth, M. Grassi, K. Ait-Oukaci, D. Stoeffler, Y. Henry, D. Lacour, M. Hehn, U. Bhaskar, M. Bailleul, T. Devolder, and J.-P. Adam, Electrical spectroscopy of forward volume spin waves in perpendicularly magnetized materials, *Phys. Rev. Res.* **2**, 043203 (2020).
- [22] M. Collet, O. Gladii, M. Evelt, V. Bessonov, L. Soumah, P. Bortolotti, S. O. Demokritov, Y. Henry, V. Cros, M. Bailleul, V. E. Demidov, and A. Anane, Spin-wave propagation in ultra-thin YIG based waveguides, *Appl. Phys. Lett.* **110**, 092408 (2017).
- [23] R. Verba, V. Tiberkevich, and A. Slavin, Wide-band nonreciprocity of surface acoustic waves induced by magnetoelastic coupling with a synthetic antiferromagnet, *Phys. Rev. Appl.* **12**, 054061 (2019).
- [24] A. F. Franco and P. Landeros, Enhancement of the spin-wave nonreciprocity in antiferromagnetically coupled multilayers with dipolar and interfacial Dzyaloshinskii-Moriya interactions, *Phys. Rev. B* **102**, 184424 (2020).
- [25] R. Gallardo, T. Schneider, A. Chaurasiya, A. Oelschlägel, S. Arekapudi, A. Roldán-Molina, R. Hübner, K. Lenz, A. Barman, J. Fassbender, J. Lindner, O. Hellwig, and P. Landeros, Reconfigurable spin-wave nonreciprocity induced by dipolar interaction in a coupled ferromagnetic bilayer, *Phys. Rev. Appl.* **12**, 034012 (2019).
- [26] M. Ishibashi, Y. Shiota, T. Li, S. Funada, T. Moriyama, and T. Ono, Switchable giant nonreciprocal frequency shift of propagating spin waves in synthetic antiferromagnets, *Sci. Adv.* **6**, eaaz6931 (2020).
- [27] F. Millo, J.-P. Adam, C. Chappert, J.-V. Kim, A. Mouhoub, A. Solignac, and T. Devolder, Unidirectionality of spin waves in synthetic antiferromagnets, *ArXiv:2306.05259* (2023).
- [28] C. Weiss, M. Bailleul, and M. Kostylev, Excitation and reception of magnetostatic surface spin waves in thin conducting ferromagnetic films by coplanar microwave antennas. Part I: Theory, *J. Magn. Magn. Mater.* **565**, 17002 (2023).
- [29] I. D. Mayergoyz, P. McAvoy, C. Tse, C. Krafft, and C. Tseng, The 2-D Hilbert transform in magnetic recording, *IEEE Trans. Magn.* **42**, 3 (2006).
- [30] We neglect the eddy currents that the antenna field generates within the magnetic film. Should the film be conductive, eddy current would partially screen the $H_z^{\text{rf}}(u, z)$ field and would smoothen its spatial profile. The sources of the magnetic field would not be located solely above the magnetic film, so that Eq. (1) would no longer strictly hold. This alteration of $H_z^{\text{rf}}(u, z)$ would quantitatively (but not qualitatively) change Eq. (9).

- [31] Equation (2) was checked to be compatible with the Maxwell-Ampere law: Its circulation about a rectilinear contour making a half turn around the antenna is $\int_{-\infty}^{+\infty} H_u^{\text{rf}}(u, z, p \rightarrow 0) du = \frac{1}{2} I \text{sgn}(z)$. Besides, Eq. (3) converges asymptotically to the well-known law: for all z , $h_z^{\text{rf}}(u \rightarrow \infty, p \rightarrow 0) = I/(2\pi u)$.
- [32] This can be checked by using Eqs. (2) and (3) and noting that $\mathcal{HT}\{\tan^{-1}(\Omega)\} = \frac{1}{2} \ln(1 + \Omega^2)$ and using the time-reversal property of the Hilbert transform (i.e., $\mathcal{HT}\{f(-\Omega)\} = -\mathcal{HT}\{f\}(-\Omega)$).
- [33] Note that the $k = 0$ case is pathological in Eq. (4) and their consequences from Eqs. (5) and (6): We have $\tilde{h}_z^{\text{rf}}(k = 0) = 0$, as this value should be the u integral of the $h_z^{\text{rf}}(u)$ field that has u -odd symmetry [see Fig. 2(a)]. Mathematically, this singularity comes from the fact that the function $h_z^{\text{rf}}(u)$ is not absolutely integrable as it asymptotically decays like $1/u$ as $u \rightarrow \pm\infty$. Physically, this singularity arises because the current in the device [Fig. 2(a), inset] flows from its source at $v = -\infty$ to $v = \infty$ without ever circulating back to its source; this singularity would be smoothed out in any real configuration because the current must return back by some path at a finite distance u_0 , leading to a $1/u^2$ decay of H_z for $|u| \gg u_0, h, w$.
- [34] They have generally different resonance frequencies and linewidths but their shapes have a high degree of similarity.
- [35] Note that an expression similar to Eq. (9) was derived in Ref. [41] for a different transducer [40] and $\varphi = \pi/2$.
- [36] A. Mouhoub, F. Millo, C. Chappert, J.-V. Kim, J. Létang, A. Solignac, and T. Devolder, Exchange energies in CoFeB/Ru/CoFeB synthetic antiferromagnets, *Phys. Rev. Mater.* **7**, 044404 (2023).
- [37] J. Mallinson, One-sided fluxes—A magnetic curiosity?, *IEEE Trans. Magn.* **9**, 678 (1973).
- [38] This expression could also have been derived directly using $\vec{\nabla} \cdot \vec{H} = 0$ outside of the film and the fact that the sole space dependence of the stray field components is its periodicity e^{-iku} and its decay $e^{-|kz|}$.
- [39] M. Johns, E. O. Fridjonsson, S. Vogt, and A. Haber, *Mobile NMR and MRI: Developments and Applications* (Royal Society of Chemistry, Cambridge, UK, 2015).
- [40] Y. Au, E. Ahmad, O. Dmytriiev, M. Dvornik, T. Davison, and V. V. Kruglyak, Resonant microwave-to-spin-wave transducer, *Appl. Phys. Lett.* **100**, 182404 (2012).
- [41] K. G. Fripp, A. V. Shytov, and V. V. Kruglyak, Spin-wave control using dark modes in chiral magnonic resonators, *Phys. Rev. B* **104**, 054437 (2021).
- [42] H. Wang, J. Chen, T. Yu, C. Liu, C. Guo, S. Liu, K. Shen, H. Jia, T. Liu, J. Zhang, M. A. Cabero, Q. Song, S. Tu, M. Wu, X. Han, K. Xia, D. Yu, G. E. W. Bauer, and H. Yu, Non-reciprocal coherent coupling of nanomagnets by exchange spin waves, *Nano Res.* **14**, 2133 (2021).
- [43] Maintaining the unitary character requires this time to take the classical definition (prefactor-free) of the Fourier transform for $\theta(k)$.
- [44] For $|r| < w$ (when the two antennas overlap) the second term on the right-hand side of Eq. (33) admits also an analytical expression (not shown, but plotted in Fig. 8).
- [45] Indeed, when $|k_0|$ is large, i.e., for frequencies obeying $|\omega - \omega_0| \gg \Delta\omega_0$, the Bedrosian theorem predicts that the $-i\mathcal{HT}$ terms in Eq. (40) will essentially vanish for $r < -w - \pi/2k_0$, as clear by comparing Figs. 9(a) and 9(b). The ripple of the envelope in Fig. 9(b) is reminiscent of the $k_0 \neq 0$ oscillations in Fig. 9(a). This nonvanishing ripple arises because the hypotheses quantitatively required to apply the Bedrosian theorem (the *disjoined* character of the spectra of the envelope and of the modulating oscillatory signal) are not strictly fulfilled.
- [46] K. Di, V. L. Zhang, H. S. Lim, S. C. Ng, M. H. Kuok, J. Yu, J. Yoon, X. Qiu, and H. Yang, Direct Observation of the Dzyaloshinskii-Moriya Interaction in a Pt/Co/Ni Film, *Phys. Rev. Lett.* **114**, 047201 (2015).
- [47] M. Belmeguenai, J.-P. Adam, Y. Roussigné, S. Eimer, T. Devolder, J.-V. Kim, S. M. Cherif, A. Stashkevich, and A. Thiaville, Interfacial Dzyaloshinskii-Moriya interaction in perpendicularly magnetized Pt/Co/AlO_x ultrathin films measured by Brillouin light spectroscopy, *Phys. Rev. B* **91**, 180405 (2015).
- [48] N. Sato, N. Ishida, T. Kawakami, and K. Sekiguchi, Propagating spectroscopy of backward volume spin waves in a metallic FeNi film, *Appl. Phys. Lett.* **104**, 032411 (2014).
- [49] P. Wessels, A. Vogel, J.-N. Tödt, M. Wieland, G. Meier, and M. Drescher, Direct observation of isolated Damon-Eshbach and backward volume spin-wave packets in ferromagnetic microstrips, *Sci. Rep.* **6**, 22117 (2016).
- [50] U. K. Bhaskar, G. Talmelli, F. Ciubotaru, C. Adelman, and T. Devolder, Backward volume vs Damon-Eshbach: A traveling spin wave spectroscopy comparison, *J. Appl. Phys.* **127**, 033902 (2020).
- [51] In practice, with a frequency $\omega - \omega_0 \gg \{\Delta\omega_0, v_g/L\}$.
- [52] We can show by numerical integration of Eq. (18) that this kind of shape is quite general and arises as soon as the dispersion relation comprises nonflat branches.
- [53] V. Vlaminck, L. Temdie, V. Castel, M. B. Jungfleisch, D. Stoeffler, Y. Henry, and M. Bailleul, Spin wave diffraction model for perpendicularly magnetized films, *J. Appl. Phys.* **133**, 053903 (2023).
- [54] M. Kiechle, A. Papp, S. Mendisch, V. Ahrens, M. Golibrzuch, G. H. Bernstein, W. Porod, G. Csaba, and M. Becherer, Spin-wave optics in YIG realized by ion-beam irradiation, *Small* **19**, 2207293 (2023).
- [55] H. Merbouche, B. Divinskiy, D. Gouéré, R. Lebrun, A. El-Kanj, V. Cros, P. Bortolotti, A. Anane, S. O. Demokritov, and V. E. Demidov, True amplification of spin waves in magnonic nano-waveguides, [ArXiv:2303.04695](https://arxiv.org/abs/2303.04695) (2023).
- [56] J. Greil, M. Golibrzuch, M. Kiechle, A. Papp, V. Ahrens, G. Csaba, and M. Becherer, Secondary excitation of spin-waves: How electromagnetic cross-talk impacts on magnonic devices, [ArXiv:2303.11303](https://arxiv.org/abs/2303.11303) (2023).